PCCP

PAPER

View Article Online
View Journal | View Issue

Cite this: *Phys. Chem. Chem. Phys.*, 2025, **27**, 22679

UV-Vis spectral simulation of polysulfur species using the nuclear ensemble approximation

Robert Skog [a] and Benjamin N. Frandsen *[ab]

Polysulfurs (S_X) are thought to be an important part of the Venusian atmospheric sulfur cycle. Among these, S_3, S_4, and S_8 have been proposed to be contributors to the enigmatic near-UV absorption feature observed between 320 and 400 nm in the atmosphere of Venus. Furthermore, the individual UV-Vis spectral signatures of polysulfur isomers remain poorly characterized, hindering the accurate photochemical modeling of these species. In this work, we use the nuclear ensemble approach to simulate the UV-Vis spectra for a comprehensive set of S_2–S_8 structural isomers, generating wavelength-dependent absolute absorption cross sections suitable for use in photochemical models. Benchmark calculations using a set of molecules and radicals were used to validate the chosen spectral simulation approach. The results show that the smaller S_2–S_4 systems have open-chain geometric isomers as their global minima, while cyclic structures are the most stable for the larger S_5–S_8 species. We also identify two low-energy triplet S_4 isomers (*cis*-$^3S_4$ and *trans*-$^3S_4$), which may serve as important intermediates. The simulated spectra indicate that the global minimum S_3 structural isomer, linear-S_3, and a high-energy structural isomer of S_4, trigonal-S_4, absorb in the 320–400 nm window, while S_8 shows negligible absorption in the 320–400 nm range. This work advances our understanding of atmospheric sulfur species beyond Earth and supports the interpretation of observations of the atmosphere of Venus and other exoplanets.

Received 5th August 2025,
Accepted 8th October 2025

DOI: 10.1039/d5cp02991k

rsc.li/pccp

1 Introduction

The atmosphere of Earth's neighboring planet Venus consists mainly of carbon dioxide (CO_2) and nitrogen (N_2), though several different sulfur-containing compounds can also be found. The most abundant sulfur species in the gas phase is sulfur dioxide (SO_2), with a mixing ratio of 100–150 ppmv around 40 km, and 10–100 ppbv between 60–85 km.[1–4] Other observed sulfur-containing species in the Venusian atmosphere include carbonyl sulfide (OCS), carbon monosulfide (CS), and carbon disulfide (CS_2).[5] Through oxidation of SO_2 and subsequent hydrolysis, sulfuric acid (H_2SO_4) is formed, which is understood to be the main component of the Venusian cloud and haze layer between 48–70 km.[1,2,4]

Atmospheric sulfur species are not limited to Venus. Using the James Webb Space Telescope, spectral signals matching SO_2 have been recorded from the atmospheres of the hot Jupiter WASP-37b,[6] the super-Neptune WASP-107b,[7] the sub-Neptune GJ 3470 b,[8] and the Super-Earth L 98-59 d.[9] Recent infrared measurements from the atmosphere of the sub-Neptune K2-18b revealed features suggested to match dimethyl sulfide (DMS) and dimethyl disulfide (DMDS), both potential biosignatures.[10] In the solar system, SO_2 was confirmed on Jupiter's moon Io using the infrared spectroscopy instrumentation onboard the Voyager 1 space probe.[11] Disulfur (S_2) was detected by the Hubble Space Telescope in the plume of Pele, a volcano on Io.[12]

In the atmosphere on Earth, sulfur species play a major role in several important atmospheric processes. The most abundant species are SO_2 and OCS, but others, such as DMS, hydrogen sulfide (H_2S), and methanesulfonic acid (MSA) are also important.[13,14] In the Venusian atmosphere SO_2 ultimately forms H_2SO_4 through oxidation and hydrolysis, and H_2SO_4 is a key contributor to acid rain[15] and atmospheric nucleation.[16–18]

Due to the relatively high mixing ratio of SO_2 in the Venusian atmosphere, it is the main absorber between 200–320 nm.[19] In addition, another weaker absorption feature can be seen in the 320–400 nm range.[20] Unfortunately, even after half a century since its discovery, there is still no scientific consensus on the identity of this unknown absorber (UA). Numerous different species have been proposed, including Cl_2,[19] SCl_2,[21] $FeCl_3$ in H_2SO_4 aerosols,[21–25] the SSCO isomer of the [C, O, S, S] system,[26] the *cis* and *trans* isomers of OSSO,[27,28] and even complex organic species formed in H_2SO_4 aerosols.[29] The latest UA candidate suggestion are different structural isomers of S_3O.[30]

[a] *Department of Chemistry, Faculty of Science, University of Helsinki, Finland. E-mail: benjamin.frandsen@helsinki.fi*
[b] *Aerosol Physics Laboratory, Faculty of Engineering and Natural Sciences, Tampere University, Finland*

One proposed set of candidate compounds as the UA are polysulfurs (S_X), specifically S_3, S_4, and S_8.[31,32] Using the data from Venera 14, Krasnopolsky[33] estimated the mixing ratio of S_3 to be (80 ± 30) ppt_V in the lower atmosphere of Venus between 5 and 25 km. By reanalyzing the spectra from Venera 11, Maiorov *et al.*[34] estimated the mixing ratio of S_3 to be 30–100 ppt_V between 3–19 km, and 0 ppt_V between 19–36 nm. Krasnopolsky[35] also reanalyzed the spectra from Venera 11, but included S_4 in the analysis. The mixing ratios of (11 ± 3) ppt_V at 3–10 km and (18 ± 3) ppt_V at 10–19 km were obtained for S_3, and (4 ± 4) ppt_V at 3–10 km and (6 ± 2) ppt_V at 10–19 km for S_4.[35] Polysulfurs are also hypothesized to be a part of the Venusian atmospheric sulfur cycle[36,37] and therefore included in several Venusian atmospheric models.[36–41] A possible polysulfur production pathway was reported by Francés-Monerris *et al.*[42] using high-level photodynamics simulations.

For S_2, quite a few studies on UV-Vis absorption have been published.[43–47] To the best of our knowledge, the most recent experimental UV-Vis spectrum of S_2 was published by Stark *et al.*[48] For the larger S_X species, Meyer *et al.*[49] identified the absorption features of S_3 and S_4 using matrix isolation spectroscopy. Later, Billmers and Smith[50] published the experimental spectra of S_3 and S_4 from sulfur vapor at 673–903 K. Hassanzadeh and Andrews[51] identified two S_4 isomers using matrix isolation spectroscopy. The absorption peak at 518 nm was assigned to the *cis* form of the linear open-chain S_4 isomer (see Fig. 1), and the peak at 560–660 nm to the cyclic-S_3 (S) isomer. Based on experimental Raman spectra of sulfur vapor, Boumedien and Picquenard[52] also assigned the peak at 560–660 nm to the cyclic-S_3 (S) isomer, but the 518 nm peak was instead attributed to the *trans* form of the open-chain isomers. Finally, Steudel *et al.*[53] measured the spectra of homocycles S_6, S_7, S_8, S_9, S_{10}, S_{12}, S_{15}, and S_{20} in solutions of methanol or methylcyclohexane.

The tendency of small polysulfur species to react and form larger ones makes it difficult to experimentally study individual structures of, for example, the S_4 system. Therefore, for distinguishing absorption features for individual isomers, a computational approach is appropriate. Several studies have investigated the excited states of S_2 using *ab initio* approaches.[54–59] Recently, Sarka *et al.*[60] performed high-level calculations and spectral simulations using the R-matrix approach for S_2, with isotopic effects included. The approach used was then further refined in a subsequent publication by Sarka and Nanbu.[61] Peterson *et al.*[62] explored the low-energy excited states of S_3 using multireference configuration interaction methods. The S_4 system was explored by Wong and Steudel,[63] who calculated vertical excitations for the different S_4 isomers. Based on these calculations, the authors concluded that the linear open-chain *cis* form of S_4 was the species absorbing at 518 nm, while the *trans* form was the absorber at 560–660 nm. Furthermore, several studies have also calculated the potential energy surfaces (PES) for different polysulfur species.[64–73]

An attractive approach for computationally simulating UV-Vis spectra for different species is the nuclear ensemble approximation (NEA). When using the NEA approach more natural absorption band widths are obtained with wavelength-dependent absolute absorption cross sections, as opposed to the stick spectra from similar vertical excitation calculations. Although the approach does not recover vibrational progression, it has been used to qualitatively reproduce the absorption spectra for a variety of species, such as sulfur-containing molecules relevant to the atmospheres of both Earth and Venus,[28,74] nucleobases,[75] isomers of Cl_2O_2,[76] the ClCO radical,[77] gaseous mercury compounds,[78] pyrrole,[79] and different volatile organic compounds.[80,81] The NEA approach was used to simulate the spectra for different UA candidates, such as the two OSSO isomers,[28] the SSCO molecule,[26] and the isomers of S_3O.[30] The approach is also used in AtmoSpec,[82] a tool for calculating photo absorption cross sections for volatile organic compounds in the troposphere of Earth.

In this work, we use the NEA approach to simulate the UV-Vis spectra for the polysulfur species S_2–S_8 to produce wavelength-dependent absolute absorption cross sections for the different species to be included in photochemical models. To confirm the validity of the chosen spectral simulation approach we performed benchmark calculations for several molecules and radicals (CS_2, H_2S, HO_2, O_3, OCS, PH_3, SO_2, and SO_3), comparing the obtained results to experimental spectra.

2 Theoretical methods

2.1 Benchmark calculations

To test the validity of the nuclear ensemble approximation method for spectral simulations of the different polysulfur species, we performed benchmark calculations using a set of molecules that have experimental spectra cataloged in the MPI-Mainz UV/VIS Spectral Atlas[83] and are small enough for high-level calculations. The molecules chosen were CS_2, H_2S, HO_2, O_3, OCS, PH_3, SO_2 and SO_3. Geometry optimizations and harmonic frequency calculations for these molecules were performed at the CCSD/aug-cc-pV(T+d)Z level of theory using the Cfour 2.1 program suite[84,85] with default convergence criteria. An unrestricted Hartree–Fock (UHF) reference was used for the HO_2 radical; for all other benchmark species, a restricted Hartree–Fock (RHF) reference was used. The frozen core approximation was employed in all coupled cluster calculations done in this work.

We performed initial test using 11 different density functionals, combined with 13 basis sets [see the SI for details]. Based on these test, we selected the overall best performing levels of theory for the benchmark calculations. The wavefunction-based method chosen was the equation-of-motion coupled cluster singles and doubles (EOM-CCSD). Farahani *et al.*[74] also found that EOM-CCSD was a good approach for accurate spectral simulation. The density functionals chosen were the hybrid GGA functional BHandHLYP,[86] the range-separated hybrid GGA functionals CAM-B3LYP[87] and ωB97X-D3,[88] and the range-separated double hybrid functional ωB2PLYP[89] without the Tamm–Dancoff approximation (TDA). In all calculations the aug-cc-pV(T+d)Z basis set[90–93] was used. EOM-CCSD calculations were performed

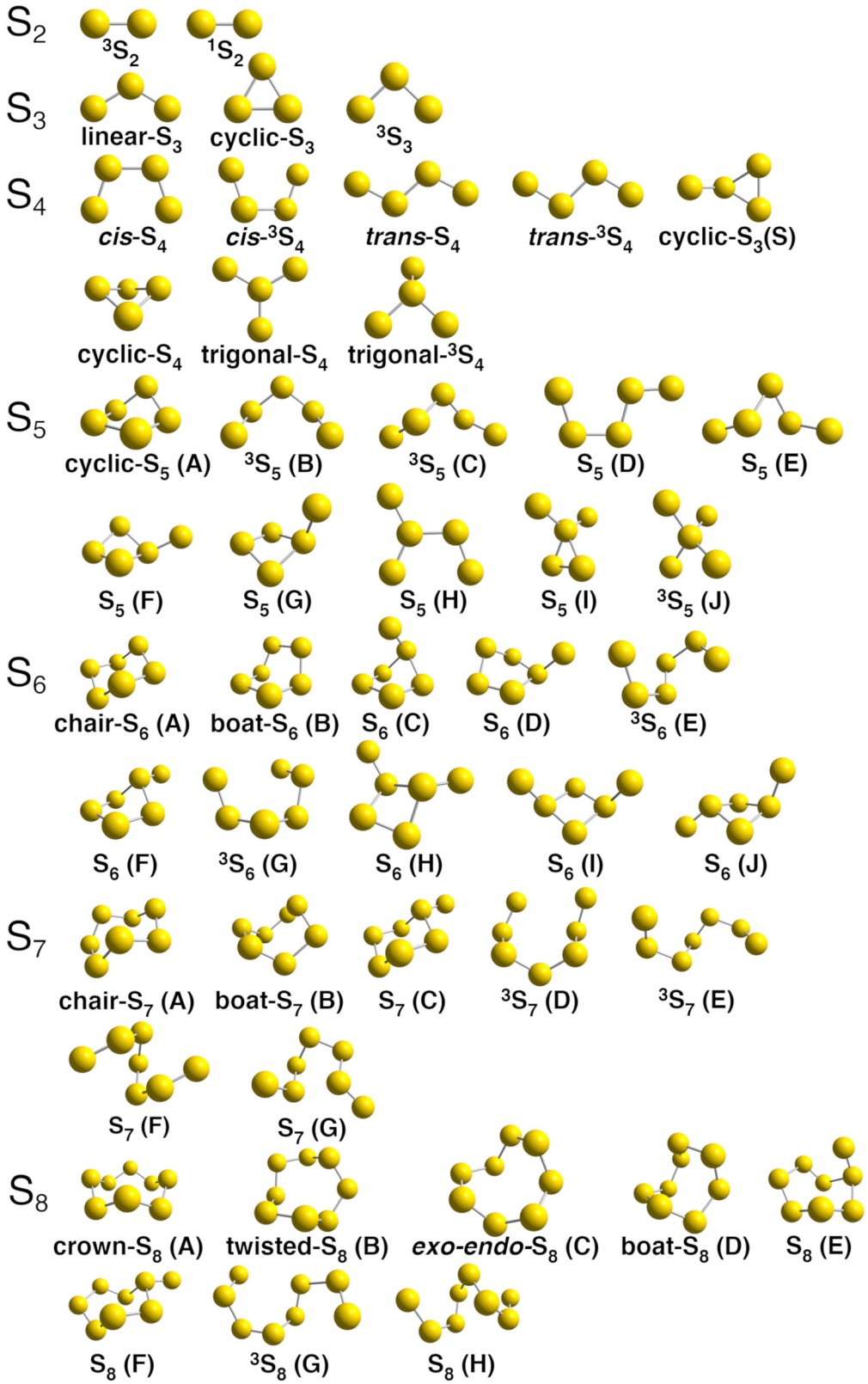

Fig. 1 All S_2–S_8 structures considered in this work, ordered by increasing zero-point vibrational corrected electronic energy.

with the Gaussian 16 Rev C.02 program.[94] All other calculations were performed with the Orca 5.0.4 quantum chemistry code.[95] The basis set exchange[96] was used to import basis sets not implemented in the quantum chemistry packages.

The theory of the nuclear ensemble approximation for spectral simulation is described in detail in the literature.[97,98] Briefly, the absorption cross section σ is calculated using eqn (1):[97]

$$\sigma(E) = \frac{\pi e^2 \hbar}{2 m_e c \varepsilon_0 n_r E} \sum_n^{N_s} \frac{1}{N_p} \sum_l^{N_p} \Delta E_{0,n}(\mathbf{R}_l) f_{0,n}(\mathbf{R}_l) g(E - \Delta E(\mathbf{R}_l), \delta_n), \quad (1)$$

where E is the photon energy, e the electron charge, m_e the electron mass, c the speed of light, ε_0 the vacuum permittivity, and n_r the refractive index. $\Delta E_{0,n}(\mathbf{R}_l)$ is the vertical excitation energy between the ground state and the excited state n with nuclear configuration $\mathbf{R}_l$. $f_{0,n}(\mathbf{R}_l)$ is the oscillator strength between the ground state and the excited state n with nuclear configuration $\mathbf{R}_l$. $g(E - \Delta E(\mathbf{R}_l), \delta_n)$ is a normalized Gaussian function, with an empirical widening of δ_n. The first sum runs over the number of excited states included (N_s), while the second sum runs over the number of geometries included in the nuclear ensemble (N_p). The vertical excitation energies and oscillator strengths are calculated with an appropriate method for each geometry in the ensemble.

In this work, the Newton-X 2.6 (build 01) program[99,100] was used for all spectral simulations. A nuclear ensemble consisting of 2000 geometries was created based on a Wigner distribution using the calculated normal modes. The ensemble size was chosen as the best compromise between minimizing the error due to statistical sampling and the computational resources needed, as shown by Farahani *et al.*[74] The ensemble size chosen in this work is also on the larger side when compared to other works using the NEA for spectral simulation.[26,30,80,101] Calculated vertical excitations were convoluted with a 0.1 eV full width at half-maximum (FWHM) normalized Gaussian function.[74] The ten lowest-energy excited states were calculated for all species. All spectral simulations were done at a temperature of 0 K. The simulated spectra were visualized using Matlab.[102]

2.2 Spectral simulations of polysulfur species

The search for stable structural isomers is trivial for S_2–S_4, since for these systems the atoms can only be arranged in a reduced number of ways. However, in the case of S_5–S_8 this becomes more difficult, especially for flexible structural isomers. Different polysulfur species previously reported in the literature were used as starting points.[64,67,69,71] For open chain structures, the Crest conformer-rotamer sampling tool[103,104] with the semi-empirical GFN2-xTB method[105] was used to find stable structures. The generated conformer ensemble obtained from the Crest search (those conformers within 6.0 kcal mol^{-1} of the lowest energy one found) was then further optimized using the ωB97X-D3 functional with the 6-31+G* basis set[106] using the Orca 5.0.4 program to obtain the final minimum energy open chain structure. All isomers/conformers identified in this work are presented in Fig. 1.

Geometry optimizations and frequency calculations for all S_2–S_8 minima and transition states were performed at the ωB97X-D/aug-cc-pV(T+d)Z[107,108] level of theory, with the Int = UltraFine and Opt = tight keywords added. Calculated normal nodes were used to verify that the optimized geometries were true minima or transition states. Intrinsic reaction coordinate (IRC) calculations were used to verify that the transition states were connected to the correct minima. In addition, the S_2–S_4 isomers were also optimized at the CCSD/aug-cc-pV(T+d)Z level of theory. Single-point energy corrections were performed at the CCSD(T)/aug-cc-pV(T+d)Z level of theory for all optimized geometries. All density functional geometry optimizations were performed with the Gaussian 16 Rev C.02 program. Coupled cluster geometry optimizations and single point energy corrections were performed with the Cfour 2.1 program suite, with the exception of the cyclic-S_4 and trigonal-$^3S_4$ structures. For these two, the Gaussian 16 Rev C.02 program was used for the CCSD/aug-cc-pV(T+d)Z geometry optimization.

Miliordos and Xantheas[109] showed that S_3 has partial biradical character. In addition, Frandsen *et al.*[27] noted that some structures of the S_2O_2 system, which is isovalent with S_4, also showed multiconfigurational character. Motivated by this, we performed additional calculations on the CCSD/aug-cc-pV(T+d)Z optimized S_2–S_4 geometries. Using the MRCC program,[110] single-point energies were calculated at the CCSDT/aug-cc-pV(T+d)Z level of theory to gauge the effect of including canonical coupled cluster triples. Complete active space self-consistent field (CASSCF) calculations, with dynamical correlation corrections accounted for with n-electron valence state perturbation theory (NEVPT2), were performed with the aug-cc-pV(T+d)Z basis set using the Orca 6.0.1 program.[111] The active spaces included all valence orbitals for the sulfur atoms, resulting in 12 electrons in 8 orbitals [CASSCF(12,8)] for S_2, CASSCF(18,12) for S_3, and CASSCF(24,16) for S_4.

For S_2–S_4, the CCSD/aug-cc-pV(T+d)Z optimized geometries and normal modes were used to create a Wigner ensemble, while ωB97X-D/aug-cc-pV(T+d)Z geometries and normal modes were used for S_5–S_8. We used the same levels of theory for the spectral simulations of the polysulfur species as in the benchmark calculations, these being EOM-CCSD, BHandHLYP, CAM-B3LYP, ωB97X-D3, and ωB2PLYP, combined with the aug-cc-pV(T+d)Z basis set. All EOM-CCSD calculations were again performed with the Gaussian 16 Rev C.02 program, and TD-DFT calculations with the Orca 5.0.4 quantum chemistry code. Spectral simulations for the S_5–S_8 species were only performed using TD-DFT, as calculations using EOM-CCSD were too computationally demanding.

To concisely communicate the levels of theory calculations were performed at we will use Method2/Basis2//Method1/Basis1 notation, where Method1/Basis1 indicates the level of theory for the geometry optimization and frequency calculation, and Method2/Basis2 refers to a single-point or vertical excitation calculation performed on the optimized geometry. If the same basis set was used in both calculations (meaning Basis1 is the same as Basis2), this is shortened to Method2//Method1/Basis1.

3 Results and discussion

3.1 Benchmark calculations

The simulated spectra for the benchmark calculations are presented in Fig. 2, and a more detailed discussion can be

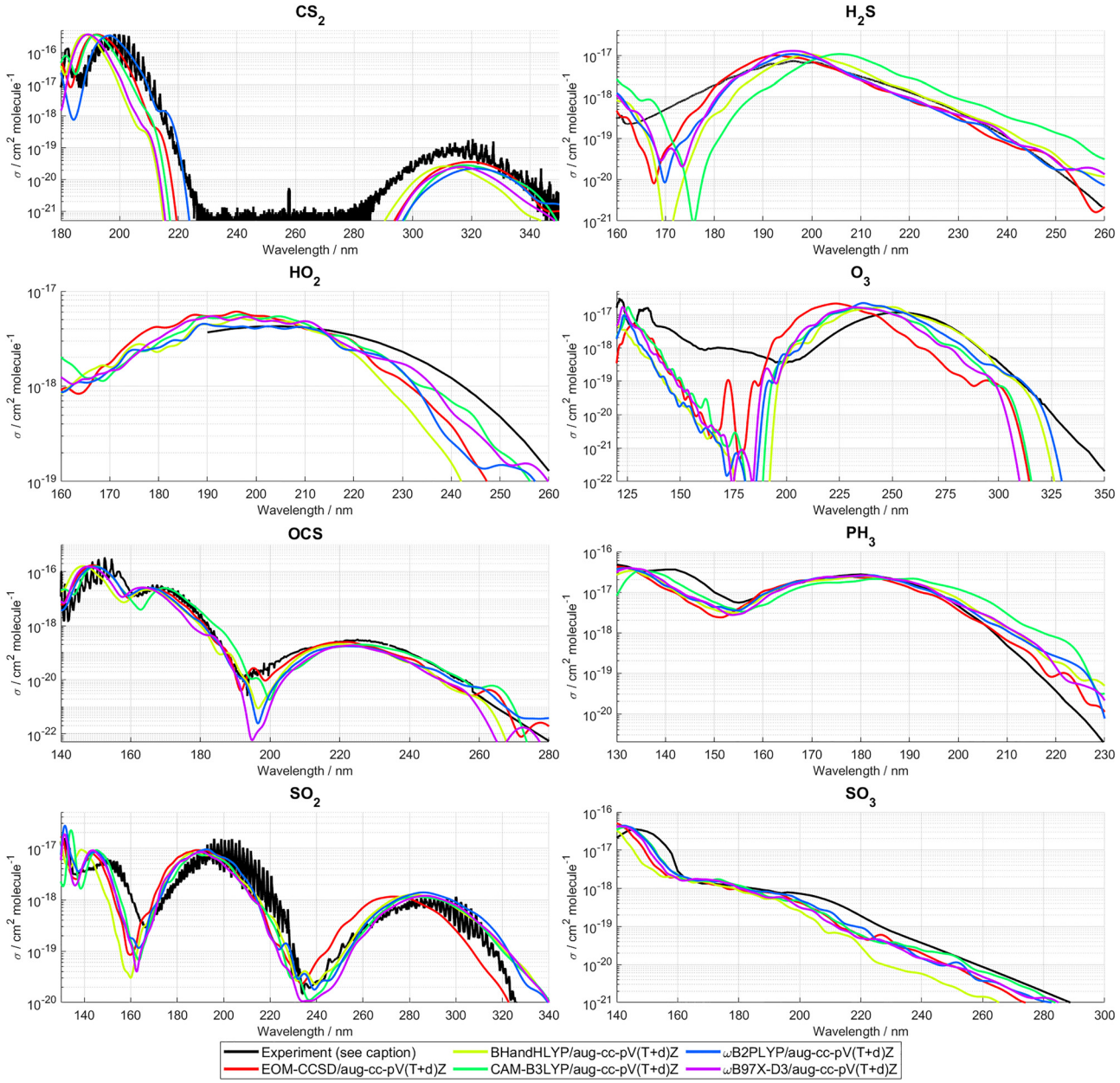

Fig. 2 The simulated spectra for the benchmark set compared to experimental spectra. Note the different scales for the axes. The references for the experimental spectra are: CS_2 – Grosch *et al.*[112] (206–350 nm), Sunanda *et al.*[113] (185–206 nm), and Rabalais *et al.*[114] (180–185 nm); H_2S – Wu and Chen[115] (160–260 nm); HO_2 – JPL 2010 recommendation[116] (160–260 nm); O_3 – JPL 2010 recommendation[116] (120–350 nm); OCS – JPL 2010 recommendation[116] (258–280 nm), Limão-Vieira *et al.*[117] (140–258 nm); PH_3 – Chen *et al.*[118] (130–230 nm); SO_2 – compilation by Manatt and Lane[119] (130–340 nm); SO_3 – Burkholder and McKeen[120] (196–300 nm), Hintze *et al.*[121] (140–194 nm).

found in the SI. Our simulated spectra capture well the overall shape of their experimental counterparts. The only noticeable exception is O_3, where a fall-off in the absorption cross section below 230 nm is seen in the simulated spectra. However, O_3 is a well-known multiconfigurational system,[109] and the spectral simulations in this work use single reference levels of theory, which explains the poor quality of the simulated spectra.

Based on the benchmark calculations and the numerous successful applications of the NEA,[26,28,30,74–76,78,80,82] we conclude that using the NEA approach to simulate the UV-Vis spectra for the different S_x species is appropriate.

3.2 Spectral simulations of polysulfur species

The relative energies for all S_2–S_8 structures considered in this work are presented in Table 1. For the spin triplet systems, where unrestricted Hartree–Fock (UHF) references were used in coupled cluster calculations, spin contamination might affect the results. To address this, we monitored the projected expectation value of the S^2 operator, $\langle S^2 \rangle$, in the UHF part of the

Table 1 Relative, zero-point vibrational energy corrected electronic energies (in kcal mol^{-1}) for the S_2–S_8 species considered in this work. All calculations use the aug-cc-pV(T+d)Z basis set, which has been omitted for brevity

	Structure	ωB97X-D[a]	CCSD(T)//ωB97X-D[a]	CCSD[a]	CCSD(T)//CCSD[a]	CCSDT//CCSD[a]	NEVPT2//CCSD[a]
S_2	$^3S_2$	0.0	0.0	0.0	0.0	0.0	0.0[b]
	$^1S_2$	22.3	17.7	19.2	17.4	16.5	13.3[b]
S_3	Linear-S_3	0.0	0.0	0.0	0.0	0.0	0.0[c]
	Cyclic-S_3	2.6	5.0	1.3	5.4	5.5	4.3[c]
	$^3S_3$	17.2	20.6	18.6	21.0	20.4	21.5[c]
S_4	*cis*-S_4	0.0	0.0	0.0	0.0	0.0	0.0[d]
	trans-S_4	8.3	8.5	8.3	8.4	7.8	8.2[d]
	cis-$^3S_4$	1.5	9.7	0.9	10.6	9.1	13.2[d]
	trans-$^3S_4$	1.8	10.9	0.9	11.3	9.8	13.7[d]
	Cyclic-S_3 (S)	7.6	12.7	7.2	13.1	—[e]	14.3[d]
	Cyclic-S_4	8.2	14.5	5.1	11.3	—[e]	17.2[d]
	Trigonal-S_4	18.5	23.5	18.9	23.7	23.2	25.2[d]
	Trigonal-$^3S_4$	38.7	46.5	39.9	47.7	45.2	49.2[d]
S_5	Cyclic-S_5 (A)	0.0	0.0				
	$^3S_5$ (B)	18.2	23.0				
	$^3S_5$ (C)	18.2	23.1				
	S_5 (D)	34.3	26.9				
	S_5 (E)	30.9	28.8				
	S_5 (F)	31.3	30.8				
	S_5 (G)	31.5	31.3				
	S_5 (H)	47.4	43.7				
	S_5 (I)	57.5	56.9				
	$^3S_5$ (J)	78.0	97.9				
S_6	Chair-S_6 (A)	0.0	0.0				
	Boat-S_6 (B)	14.3	13.2				
	S_6 (C)	29.3	23.5				
	S_6 (D)	27.0	24.2				
	$^3S_6$ (E)	27.8	29.1				
	S_6 (F)	32.6	29.3				
	$^3S_6$ (G)	28.7	32.2				
	S_6 (H)	48.2	43.8				
	S_6 (I)	54.2	51.3				
	S_6 (J)	56.5	53.5				
S_7	Chair-S_7 (A)	0.0	0.0				
	Boat-S_7 (B)	5.8	4.2				
	S_7 (C)	21.2	19.1				
	$^3S_7$ (D)	29.0	32.5				
	$^3S_7$ (E)	28.9	33.1				
	S_7 (F)	45.0	35.5				
	S_7 (G)	42.2	36.0				
S_8	Crown-S_8 (A)	0.0	0.0				
	Twisted-S_8 (B)	10.4	8.8				
	exo–endo-S_8 (C)	11.4	9.7				
	Boat-S_8 (D)	21.2	17.0				
	S_8 (E)	25.7	18.3				
	S_8 (F)	30.8	26.6				
	$^3S_8$ (G)	36.4	37.4				
	S_8 (H)	68.1	49.2				

[a] See the end of Section 2.2 for an explanation of the convention used to indicate the level of theory used. [b] Calculated using NEVPT2(12,8) on top of a CASSCF(12,8) reference. [c] Calculated using NEVPT2(18,12) on top of a CASSCF(18,12) reference. [d] Calculated using NEVPT2(24,16) on top of a CASSCF(24,16) reference. [e] Calculation did not converge.

coupled cluster calculations. For a triplet system, the ideal $\langle S^2 \rangle$ value is 2.00. The highest value was found for structure $^3S_5$ (J), with $\langle S^2 \rangle$ = 2.11. While this is somewhat high, $^3S_5$ (J) is a relatively high energy S_5 species. All other structures had a $\langle S^2 \rangle$ value lower than 2.09, which we still consider acceptable.

Below we discuss the results for the different S_X systems in more detail.

3.2.1 S_2. Analogously to O_2, the ground state of S_2 has triplet multiplicity. The experimental energy difference between the singlet and triplet structures used in the work by Swope *et al.*[54] is 13.4 kcal mol^{-1}. However, Barnes *et al.*[122] reported the energy difference as 16.4 kcal mol^{-1}. Calculated energy differences range between 12.4 and 15.8 kcal mol^{-1}.[54,55,57,123] As seen in Table 1, the NEVPT2(12,8)//CCSD/aug-cc-pV(T+d)Z energy is more in line with the experimental value used by Swope *et al.*,[54] while the CCSDT//CCSD/aug-cc-pV(T+d)Z, CCSD(T)//CCSD/aug-cc-pV(T+d)Z, and CCSD(T)//ωB97X-D/aug-cc-pV(T+d)Z levels of theory align better with the result by Barnes *et al.*[122] Based on the configuration state function (CSF) weights of the single-point NEVPT2(12,8)//CCSD/aug-cc-pV(T+d)Z calculations, shown in Table A1 in the SI, static correlation plays a significant role, especially for the singlet state. Therefore, we consider

the 13.3 kcal mol^{-1} energy gap, calculated at the NEVPT2 (12,8)//CCSD/aug-cc-pV(T+d)Z level of theory, to be the more accurate value.

A high-resolution UV-Vis spectrum of S_2 was recently published by Stark *et al.*[48] Therefore, we present our simulated spectra in Fig. A9 in the SI. The simulated spectra do not reproduce the vibrational fine structure seen in the experimental spectrum due to neglecting Franck–Condon factors.

3.2.2 S_3. There are two minima on the singlet S_3 potential energy surface (PES): linear-S_3 and cyclic-S_3. By analyzing the rotational spectrum of S_3, McCarthy *et al.*[124] and Thorwirth *et al.*[125] derived the experimental structural parameters for linear-S_3. Calculations by Raghavachari *et al.*[66] showed that linear-S_3 was the global minimum energy structural isomer. Peterson *et al.*[62] reached the same conclusion, as they calculated cyclic-S_3 to be (4.4 ± 0.5) kcal mol^{-1} higher in energy than linear-S_3. As seen in Table 1, we also find that linear-S_3 is the minimum energy isomer. Energies calculated in this work at the CCSD/aug-cc-pV(T+d)Z and ωB97X-D/aug-cc-pV(T+d)Z levels of theory somewhat underestimate the difference between linear-S_3 and cyclic-S_3, but the other levels of theory are in good agreement. As seen in Table A2 in the SI, based on the CSF weights, the S_3 structures show some multiconfigurational character. Due to this finding, using the NEVPT2(18,12)//CCSD/aug-cc-pV(T+d)Z relative energy is recommended. Also notable is the fact that the isomerization reaction connecting

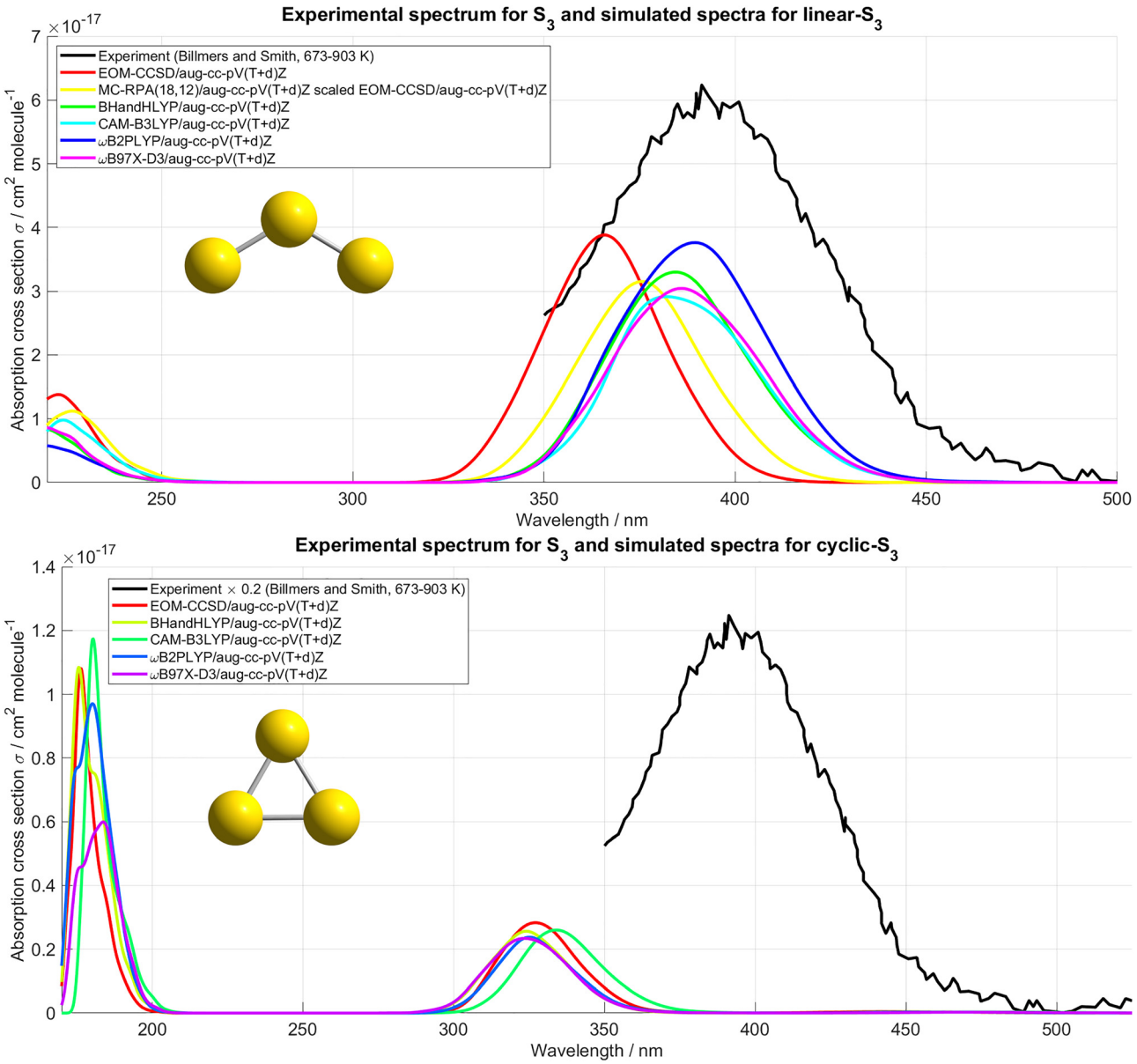

Fig. 3 Simulated spectra for the two singlet S_3 isomers, compared with the experimental spectrum of S_3 by Billmers and Smith,[50] measured at temperatures in the range of 673–903 K. The experimental spectrum was digitized using the PlotDigitizer[134] tool. Note the different scales on the axes. The experimental spectrum has been scaled down by 80% for clarity in the lower part of the figure.

the two minima is orbital-symmetry-forbidden,[126] having a barrier of about 27.6–29.4 kcal mol^{-1}.[127,128]

The simulated spectra for the S_3 isomers are presented in Fig. 3. For the cyclic-S_3 isomer, all simulated spectra are in good agreement with each other. However, with the linear-S_3 isomer, a blue shift in the EOM-CCSD/aug-cc-pV(T+d)Z simulated spectrum is observed when compared to the TD-DFT spectra. To investigate this discrepancy, we performed further single-point vertical excitation calculations on the CCSD/aug-cc-pV(T+d)Z optimized geometry. The vertical excitation energies and oscillator strengths for the three lowest energy excited states were calculated using multiconfigurational random phase approximation, MC-RPA(18,12)/aug-cc-pV(T+d)Z, on top of a CASSCF(18,12)/aug-cc-pV(T+d)Z reference using the Orca 6.0.1 program.[111] The MC-RPA approach was chosen based on its reasonable computational cost and relatively good performance compared to other multireference methods.[129,130] Furthermore, EOM-CC3/aug-cc-pV(T+d)Z vertical excitation calculations were performed using the e^T 1.9.13 program.[131]

The results from these additional calculations are presented in Table A4 in the SI. When specifically looking at the third transition ($S_3 \leftarrow S_0$), the result from the EOM-CCSD/aug-cc-pV(T+d)Z calculation is slightly better in line with the MC-RPA(18,12)/aug-cc-pV(T+d)Z and EOM-CC3/aug-cc-pV(T+d)Z results. Using the MC-RPA(18,12)/aug-cc-pV(T+d)Z results, we scale the EOM-CCSD/aug-cc-pV(T+d)Z simulated spectrum and visualize this in Fig. 3, which we recommend as our highest quality linear-S_3 UV-Vis spectrum (the scaling procedure is outlined in Section A2.3 in the SI). Scaling based on the MR-RPA result was motivated by the non-negligible amount of multiconfigurational character present in linear-S_3. For cyclic-S_3 we recommend the EOM-CCSD/aug-cc-pV(T+d)Z spectrum.

All simulated spectra in Fig. 3 predict a lower absorption cross section than the experimental spectrum. This is especially relevant for linear-S_3, as this is the minimum energy isomer. However, it should be noted that the experimental spectrum was measured at very high temperatures, 673–903 K.[50] Therefore, we postulate that the primary difference between the experimental spectrum and the simulated spectra originates from the different temperatures used, such as by the inclusion of hot bands in the experimental spectrum. Because of the high temperatures used in the experimental work, we consider the simulated spectra to be representative of a lower temperature (0–300 K) absorption spectra for use in photochemical models.

S_3 was one of the polysulfur species suggested as the unknown absorber (UA).[32] Indeed, based on our simulated spectra, linear-S_3 absorbs in the same wavelength region as the UA (320–400 nm) with a relatively large absorption cross section. But the spectral match is only one part, as there must also be an appreciable abundance of linear-S_3 in the Venusian atmosphere to have an impact. The model by Zhang *et al.*[37] predicts a S_3 mixing ratio of approximately 0.01 ppt_v at an altitude of 58 km. However, while accurate reaction rates have been calculated for the S + S_2 reaction,[132] other reaction rates for polysyulfurs are still based on estimates.[133] Updated reaction rates are needed for a more accurate determination.

3.2.3 S_4. There are several minima on the S_4 PES. While most studies agree that the global minimum of S_4 is the *cis* form of the linear open chain structures (*cis*-S_4 in Fig. 1),[63,65,66,72] some report a rectangular structure to be the global minimum.[71,135]

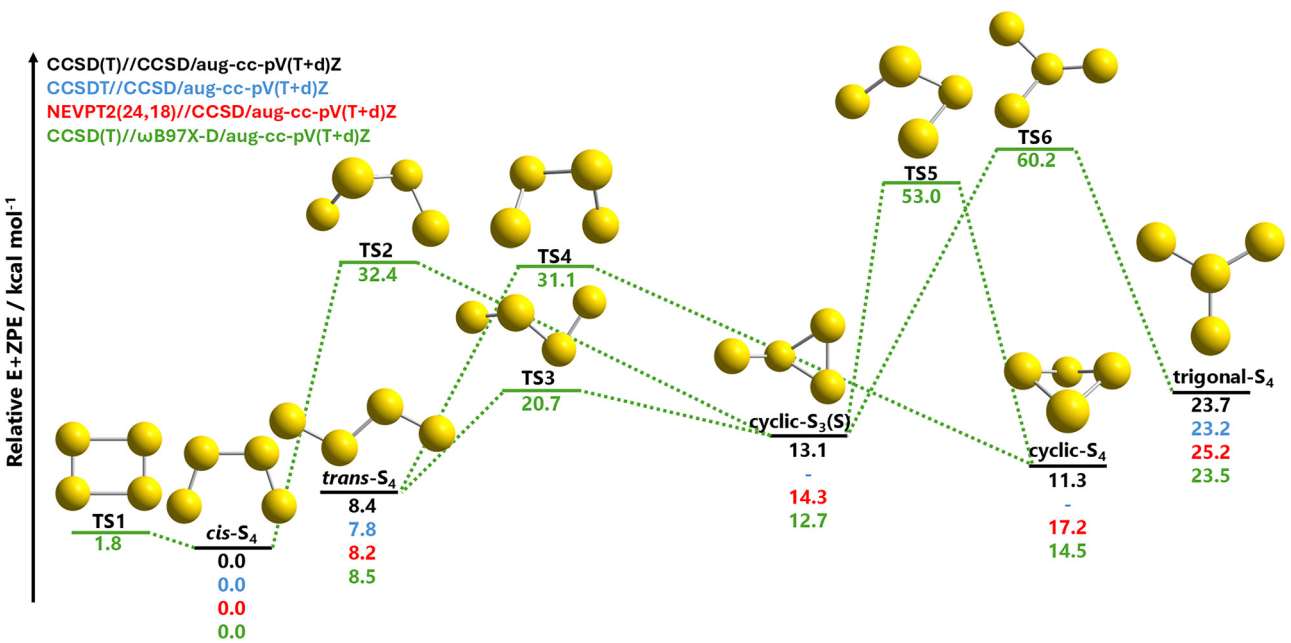

Fig. 4 The singlet potential energy surface (PES) for the S_4 system. Energies are relative zero-point vibrational energy corrected electronic energies (kcal mol^{-1}). The coloring corresponds to the level of theory used: black – CCSD(T)//CCSD/aug-cc-pV(T+d)Z; blue – CCSDT//CCSD/aug-cc-pV(T+d)Z; red – NEVPT2(24,16)//CCSD/aug-cc-pV(T+d)Z; green – CCSD(T)//ωB97X-D/aug-cc-pV(T+d)Z. Note that the calculations using CCSDT//CCSD/aug-cc-pV(T+d)Z did not converge for the cyclic-S_3 (S) and cyclic-S_4 structures.

Our results agree with the former, as we predict *cis*-S_4 to be the lowest energy isomer, being approximately 8 kcal mol^{-1} lower in energy than the linear open-chain *trans* structure. Thorwirth *et al.*[125] also identified *cis*-S_4 through rotational spectroscopy. Curiously, we found that the energy differences between the singlet and triplet linear open-chain *cis* and *trans* structures are quite small when using the ωB97X-D/aug-cc-pV(T+d)Z and CCSD/aug-cc-pV(T+d)Z levels of theory. However, when adding energy corrections using CCSD(T)/aug-cc-pV(T+d)Z, CCSDT/aug-cc-pV(T+d)Z, and NEVPT2(24,16)/aug-cc-pV(T+d)Z, the energy differences increase, yet remain below 15 kcal mol^{-1}, as seen in Table 1.

The singlet PES for the S_4 system is shown in Fig. 4. We find, like Wong and Steudel,[63] that the rectangular structure (labeled TS1 in Fig. 4) is a transition state. At the ωB97X-D/aug-cc-pV(T+d)Z level of theory this transition state corresponds to an interconversion of *cis*-S_4 to itself, which might be relevant for isotope scrambling. We also note that, despite our best efforts, we were unable to locate a transition state connecting *cis*-S_4 to *trans*-S_4 at the ωB97X-D/aug-cc-pV(T+d)Z level of theory. As can be seen in Table A3 in the SI, the CSF weights of *cis*-S_4 and *trans*-S_4 indicate that multiconfigurational approaches should be used. Therefore, this transition state might exist only on a multireference PES, or proceed *via* the spin triplet PES. However, based on the relatively high isomerization energies shown in Fig. 4, we conclude, as did Wong and Steudel,[63] that the different singlet structural isomers are well

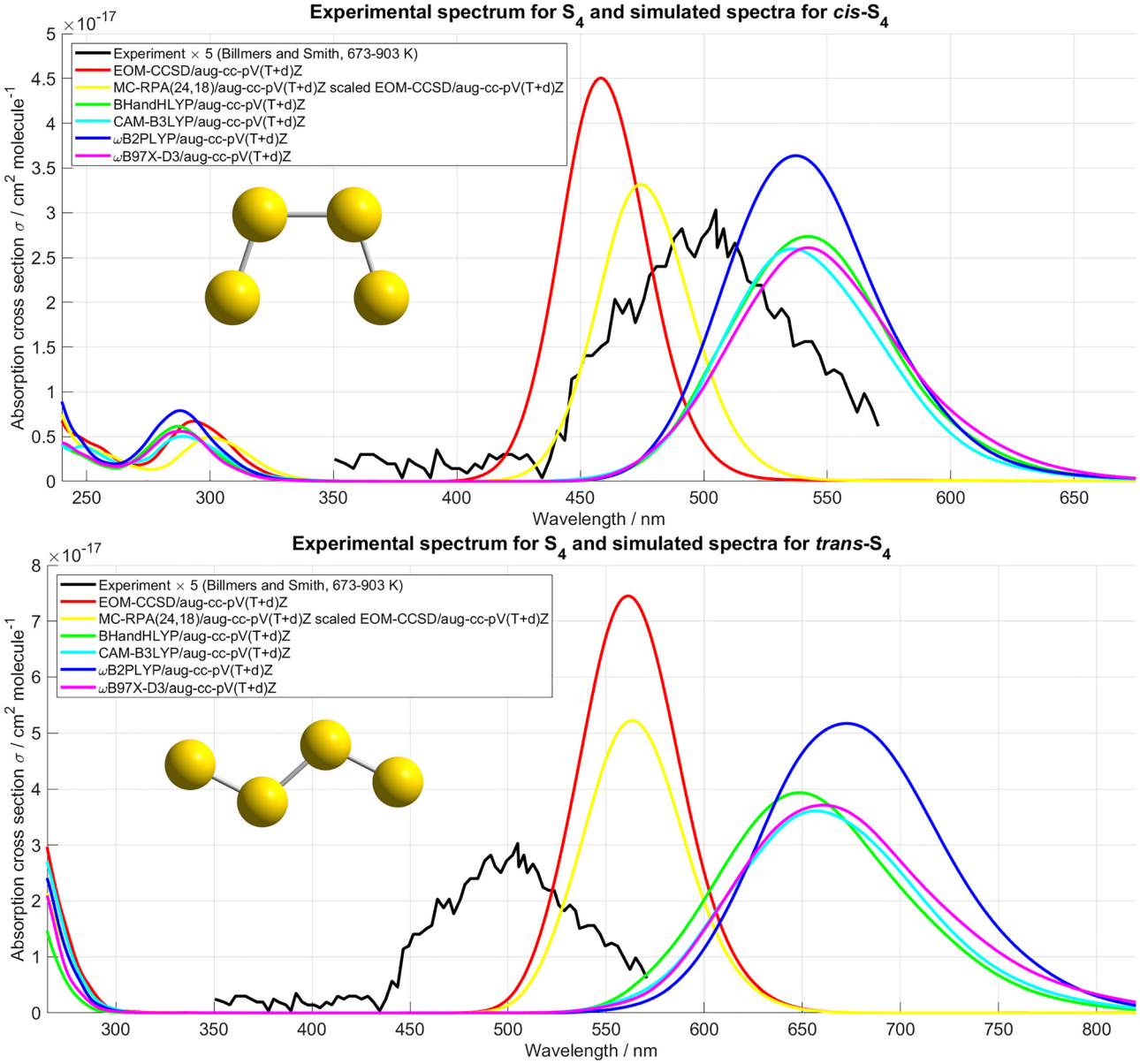

Fig. 5 Simulated spectra for *cis*-S_4 and *trans*-S_4, compared with the scaled experimental spectrum of S_4 by Billmers and Smith,[50] measured at temperatures in the range of 673–903 K. The experimental spectrum was digitized using the PlotDigitizer[134] tool. The experimental spectrum has been scaled up by 400% for clarity. Note the different scales on the axes.

separated and should be experimentally accessible, especially in low-temperature conditions.

The simulated spectra for the S_4 singlet species are presented in Fig. 5–7. The simulated spectra for cyclic-S_3 (S), cyclic-S_4, and trigonal-S_4 are similar. But for *cis*-S_4 and *trans*-S_4, the first peak in the EOM-CCSD/aug-cc-pV(T+d)Z spectra is blue-shifted compared to the spectra simulated using TD-DFT. Therefore, as with linear-S_3, we performed additional vertical excitation calculations on the CCSD/aug-cc-pV(TT+d)Z optimized geometries using EOM-CC3/aug-cc-pV(T+d)Z and MC-RPA(24,16)/aug-cc-pV(T+d)Z.

The vertical excitation energies and oscillator strengths for the three lowest excited states of *cis*-S_4 and *trans*-S_4 are presented in the SI in Tables A5 and A6. It is clear that the vertical excitation energies calculated at the EOM-CCSD/aug-cc-pV(T+d)Z level of theory are in good agreement with those calculated using EOM-CC3/aug-cc-pV(T+d)Z and MC-RPA(24,16)/aug-cc-pV(T+d)Z. In contrast, TD-DFT energies differ by approximately 100 nm. We use the results from the MC-RPA(24,16)/aug-cc-pV(T+d)Z calculations and scale the EOM-CCSD/aug-cc-pV(T+d)Z spectra for both *cis*-S_4 and *trans*-S_4. These scaled spectra are also visualized in Fig. 5, and we recommend these as our highest quality UV-Vis spectra for *cis*-S_4 and *trans*-S_4 to be used in photochemical models. The EOM-CCSD/aug-cc-pV(T+d)Z spectra are recommended for the other singlet S_4 isomers.

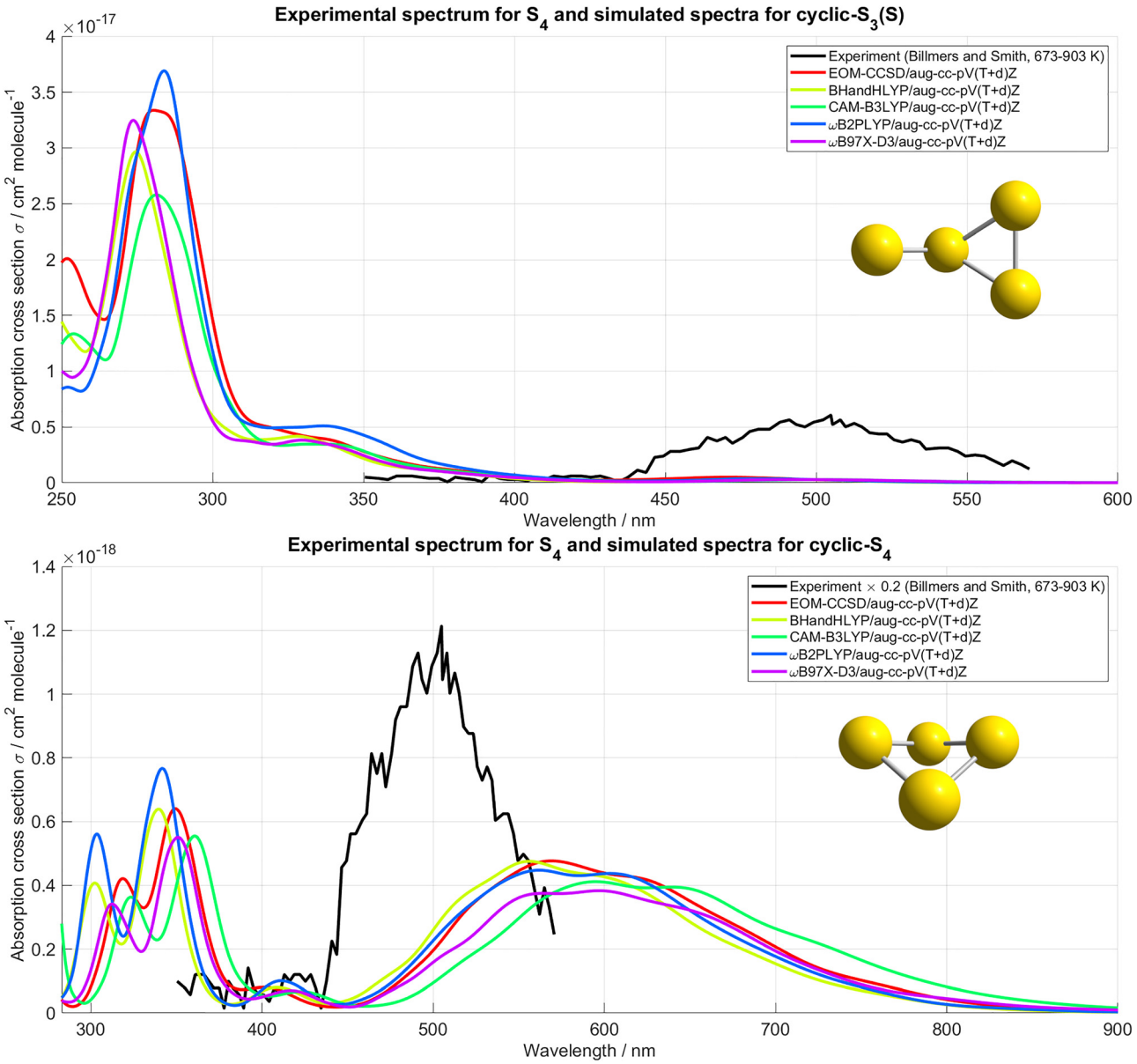

Fig. 6 Simulated spectra for cyclic-S_3 (S) and cyclic-S_4, compared with the experimental spectrum of S_4 by Billmers and Smith,[50] measured at temperatures in the range of 673–903 K. The experimental spectrum was digitized using the PlotDigitizer[134] tool. Note the different scales on the axes. The experimental spectrum has been scaled down by 80% for clarity in the lower part of the figure.

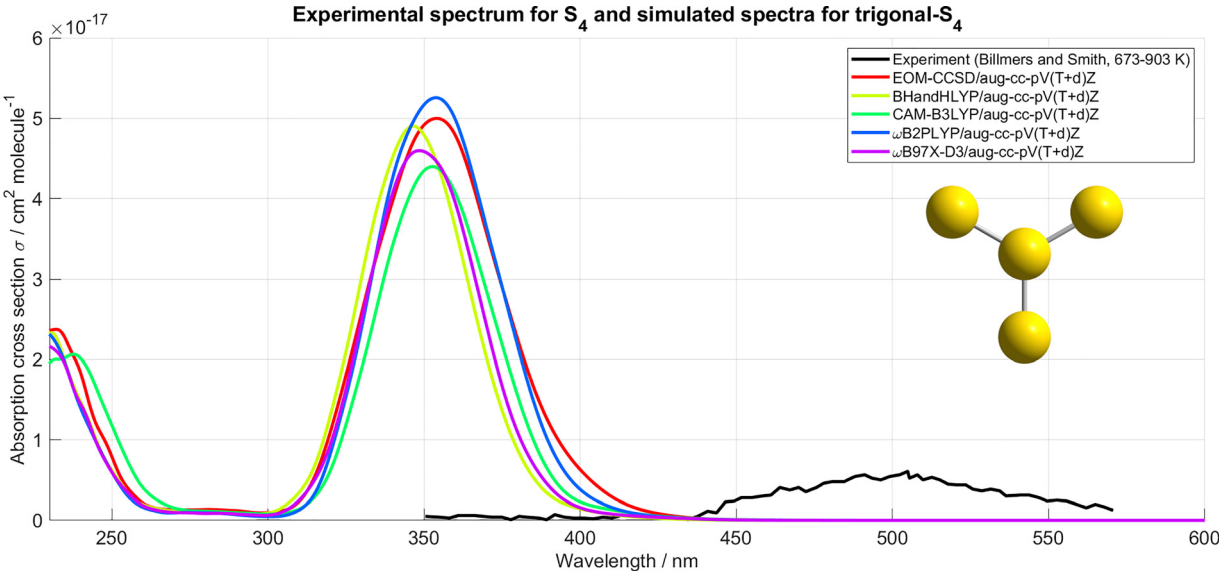

Fig. 7 Simulated spectra for trigonal-S_4, compared with the experimental spectrum of S_4 by Billmers and Smith,[50] measured at temperatures in the range of 673–903 K. The experimental spectrum was digitized using the PlotDigitizer[134] tool.

In Fig. 8 we show the simulated spectra for the spin triplet S_4 species *cis*-$^3S_4$ and *trans*-$^3S_4$. In the case of *cis*-$^3S_4$, simulated spectra are similar, except for the ωB2PLYP/aug-cc-pV(T+d)Z spectrum. The ωB2PLYP/aug-cc-pV(T+d)Z spectrum is more uniform, while the other simulated spectra show two different peaks. The ωB2PLYP/aug-cc-pV(T+d)Z spectrum also predicts a larger absorption cross section. For *trans*-$^3S_4$, all simulated spectra are similar. Furthermore, as can be seen and Fig. A10 and A11 in the SI, the simulated spectra predict that the triplet S_4 species weakly absorb in the near-infrared region.

Of the S_4 isomers we have studied in this work, based on the simulated spectra, we find that trigonal-S_4 absorbs in the same wavelength window as the UA. Furthermore, the triplet structures *cis*-$^3S_4$ and *trans*-$^3S_4$ also show some absorption between 320 and 400 nm. However, *cis*-$^3S_4$ and *trans*-$^3S_4$ are very unlikely to contribute to the enigmatic absorption, but they might be a useful addition as intermediates in photochemical models. Zhang *et al.*[37] estimated a mixing ratio of approximately 0.1 ppt_V using their Venusian atmospheric model. However, the reaction rates are again based on estimates.[133] In addition, atmospheric models do not differentiate between the S_4 species.[36–41] Based on the PES in Fig. 4, the S_4 isomers are separated by quite high barriers, meaning that several isomers could form and persist. Therefore, individual reaction rates for the formation and consumption of the different isomers should be determined.

3.2.4 S_5–S_8. The number of possible minima for the S_5–S_8 systems are greater than for S_2–S_4, simply because of the increased number of atoms in the system. However, when looking at Table 1 a clear trend is seen; the cyclic structures are the lowest energy structural isomers. Still, the higher energy S_5–S_8 structures might be important intermediates in polysulfur reactions. We simulate the UV-Vis spectra for the lowest energy S_5–S_8 isomers and those isomers found in Table 1 within 5.0 kcal mol^{-1} of the lowest energy one. Because these structures are closed-shell singlet species, we believe TD-DFT is an appropriate level of theory for the spectral simulations. The results of these spectral simulations are presented in Fig. 9–12.

The cyclic-S_5 structure is clearly the most stable S_5 structural isomer, being 20 kcal mol^{-1} lower in energy than the next lowest energy S_5, which is $^3S_5$ (B). To the best of knowledge, no experimental UV-Vis spectrum for S_5 has been published. As seen in Fig. 9, three of the TD-DFT methods, BHandLHYP/aug-cc-pV(T+d)Z, CAM-B3LYP/aug-cc-pV(T+d)Z, and ωB97X-D3/aug-cc-pV(T+d)Z, predict similar absorption profiles for cyclic-S_5, with a maximum around 290 nm. The ωB2PLYP/aug-cc-pV(T+d)Z spectrum differs slightly from the others. Although there is a clear shoulder around 290 nm, the maximum is predicted to be at 265 nm.

Like cyclohexane, there are two different conformers of cyclic S_6. Of these two, the chair conformer is the minimum, as the boat conformer is calculated to be 13.2 kcal mol^{-1} higher in energy at the CCSD(T)//ωB97X-D/aug-cc-pV(T+d)Z level of theory. This is in excellent agreement with the energy difference reported by Cioslowski *et al.*[68] Other studies also report chair-S_6 to be the minimum energy structure.[66,71] The experimental spectrum of S_6 by Steudel *et al.*[53] seen in Fig. 10 shows a steady increase in the absorption cross section when going below 330 nm. All simulated spectra predict a lower absorption cross section than the experiment, but the steady increase is reproduced.

For S_7, the general features of the experimental spectrum are similar to that of S_6; at wavelengths shorter than 340 nm, the absorption cross section steadily increases. Spectral simulations were performed for two structures, these being chair-S_7 and boat-S_7, as the energy difference is only 4.2 kcal mol^{-1} at the CCSD(T)//ωB97X-D/aug-cc-pV(T+d)Z level of theory – an energy gap consistent with previous results.[66,68,71] The simulated spectra in

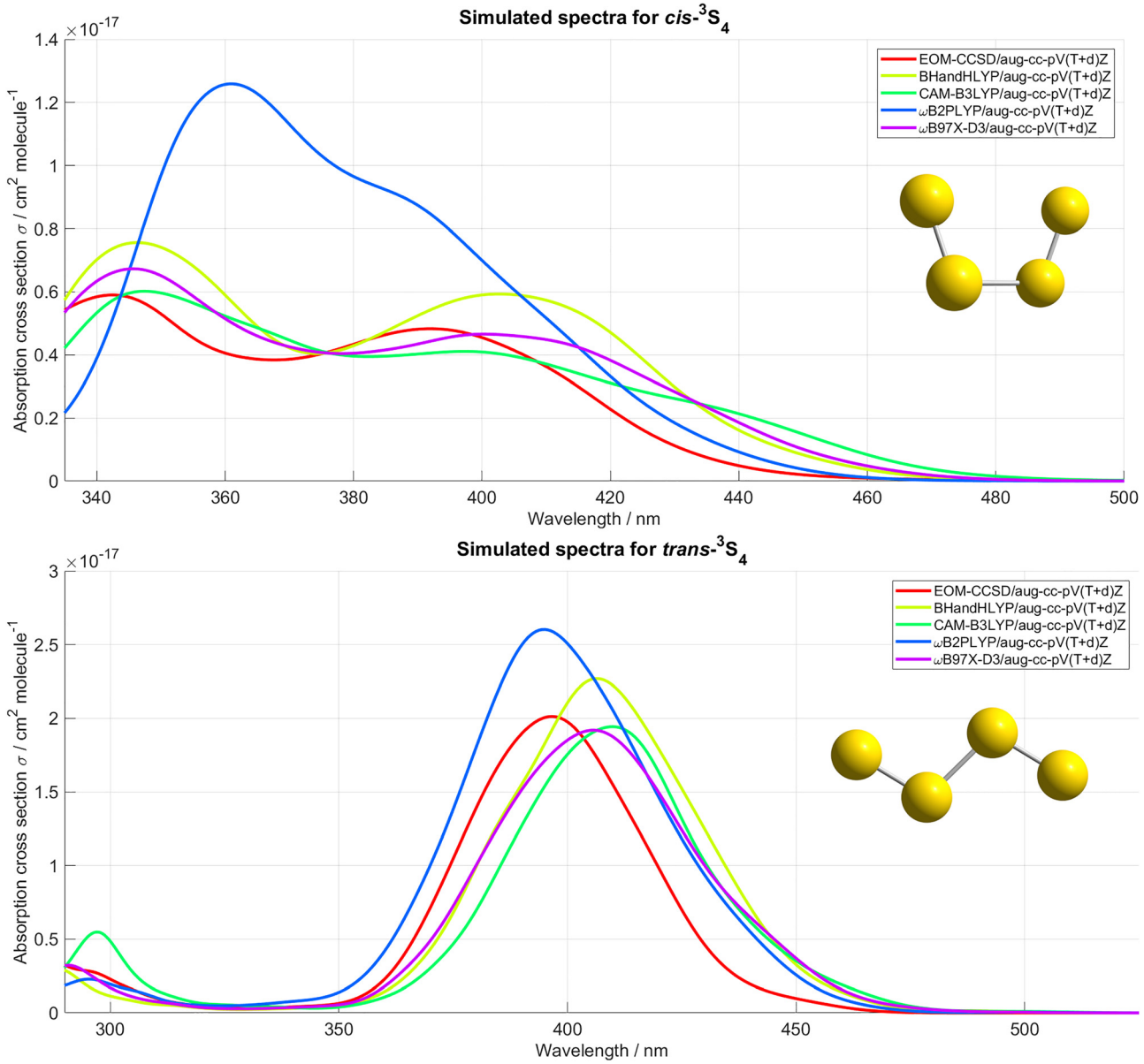

Fig. 8 Simulated spectra for *cis*-$^3S_4$ and *trans*-$^3S_4$. Note the different scales on the axes.

Fig. 11 show a lower absorption cross section compared to the experimental counterpart, but once again the general shape is reproduced. The overall absorption cross section of the boat-S_7 conformer is predicted to be slightly higher than that of the chair-S_7 conformer, even surpassing the experimental value below 270 nm.

There are several unique cyclic S_8 structures. Our calculations show that the lowest energy structure is crown-S_8, which is consistent with previously reported results.[66–68,70,71] Contrary to the findings by Wong *et al.*,[70] we find that the twisted-S_8 is slightly lower in energy compared to the *exo–endo*-S_8 conformer. Using simulated annealing, Jones and Hohl[135] reported a S_8 cluster (see Fig. 1b in ref. 135) that was only 9.9 kcal mol^{-1} higher in energy than crown-S_8. This cluster was also reported by Wong *et al.*[70] and Jones and Ballone.[71] However, using ωB97X-D/aug-cc-pV(T+d)Z, this cluster optimizes to the S_8 (E) structure, which is 18.3 kcal mol^{-1} higher in energy than crown-S_8 at the CCSD(T)//ωB97X-D/aug-cc-pV(T+d)Z level of theory. The experimental spectrum for S_8 is presented in Fig. 12, together with the simulated spectra for crown-S_8. The simulated spectra predict a lower absorption cross section compared to the experimental spectrum between 320–270 nm, but reach agreement at 260 nm.

An important detail with respect to the experimental UV-Vis spectra published by Steudel *et al.* used for S_6–S_8 is that these are liquid phase spectra, measured in methylcyclohexane (C_7H_{14}). Different effects, such as clustering or solvent interactions, might affect the final spectrum. In contrast, our simulated spectra are in the gas phase. Therefore, the experimental spectra are not directly comparable to our spectra. We consider

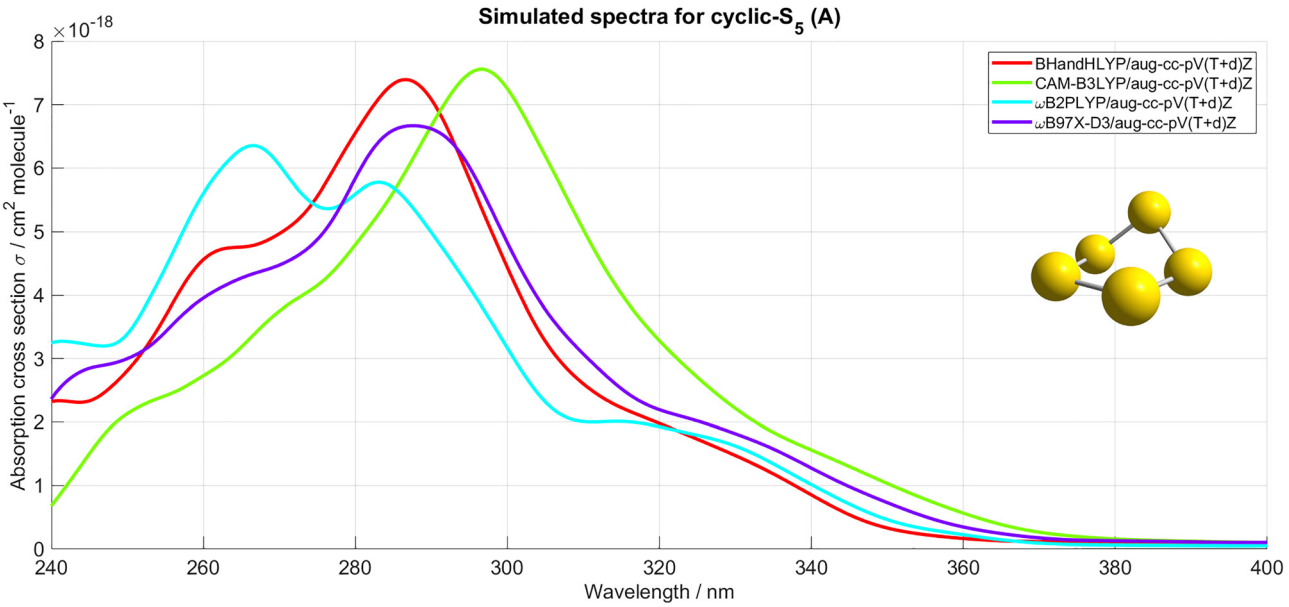

Fig. 9 The simulated spectra for cyclic-S_5 (A).

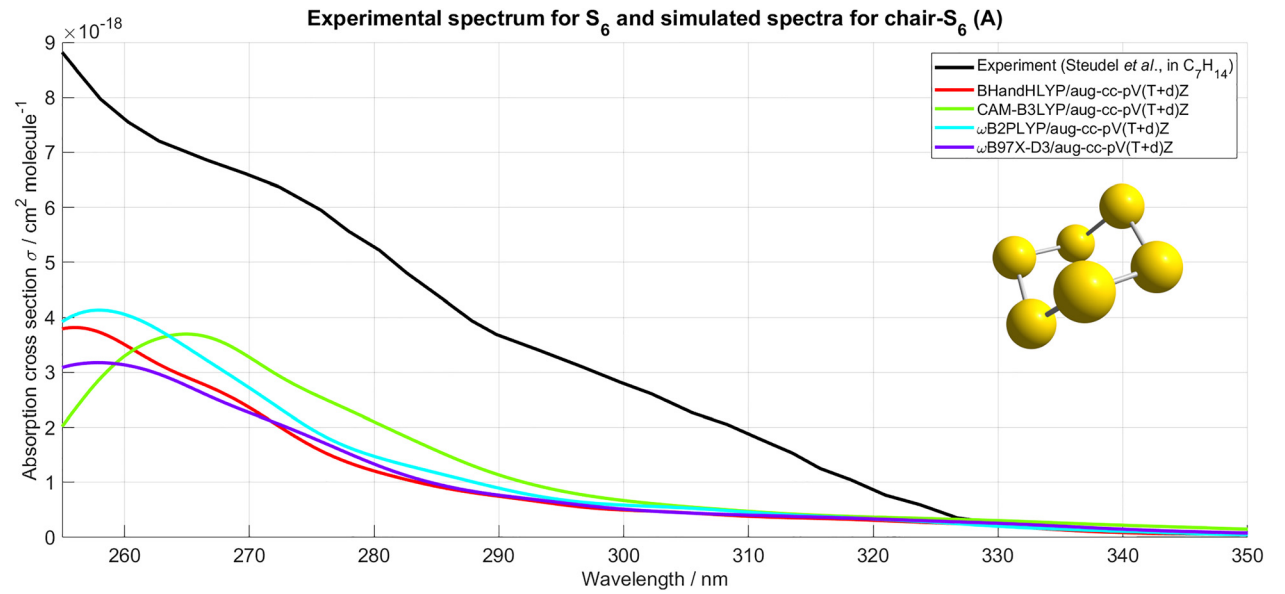

Fig. 10 The simulated spectra for chair-S_6, compared to the experimental spectrum by Steudel *et al.*[53] measured in a methylcyclohexane (C_7H_{14}) solution. The experimental spectrum was digitized using the PlotDigitizer[134] tool.

our simulated spectra to be a more appropriate representation of gas phase spectra. For the S_5–S_8 species, we recommend using the spectra simulated at the ωB97X-D3/aug-cc-pV(T+d)Z level of theory.

The experimental spectra S_6–S_8 reach down to approximately 220 nm. To construct the simulated spectra, we used the ten lowest excited states. This number of excited states limits us to about 250–260 nm. Increasing the number of excited states would extend the simulated spectra, but this was prohibitively expensive and thus not done in this work.

We estimated if spin–orbit coupling (SOC) would influence the simulated spectra in any significant way. We performed single-point vertical excitation calculations using the ωB97X-D3 functional with the aug-cc-pV(T+d)Z basis set on the ωB97X-D/aug-cc-pV(T+d)Z optimized geometries [specifically, linear-S_3, cyclic-S_3, *cis*-S_4, *trans*-S_4, cyclic-S_5 (A), chair-S_6 (A), chair-S_7 (A), boat-S_7 (B), and crown-S_8 (A)]. The calculations were performed with the Orca 6.0.1 program, where SOC is implemented for TD-DFT.[136] We saw shifts of less than 0.02 eV when comparing the calculated singlet transitions without SOC with those

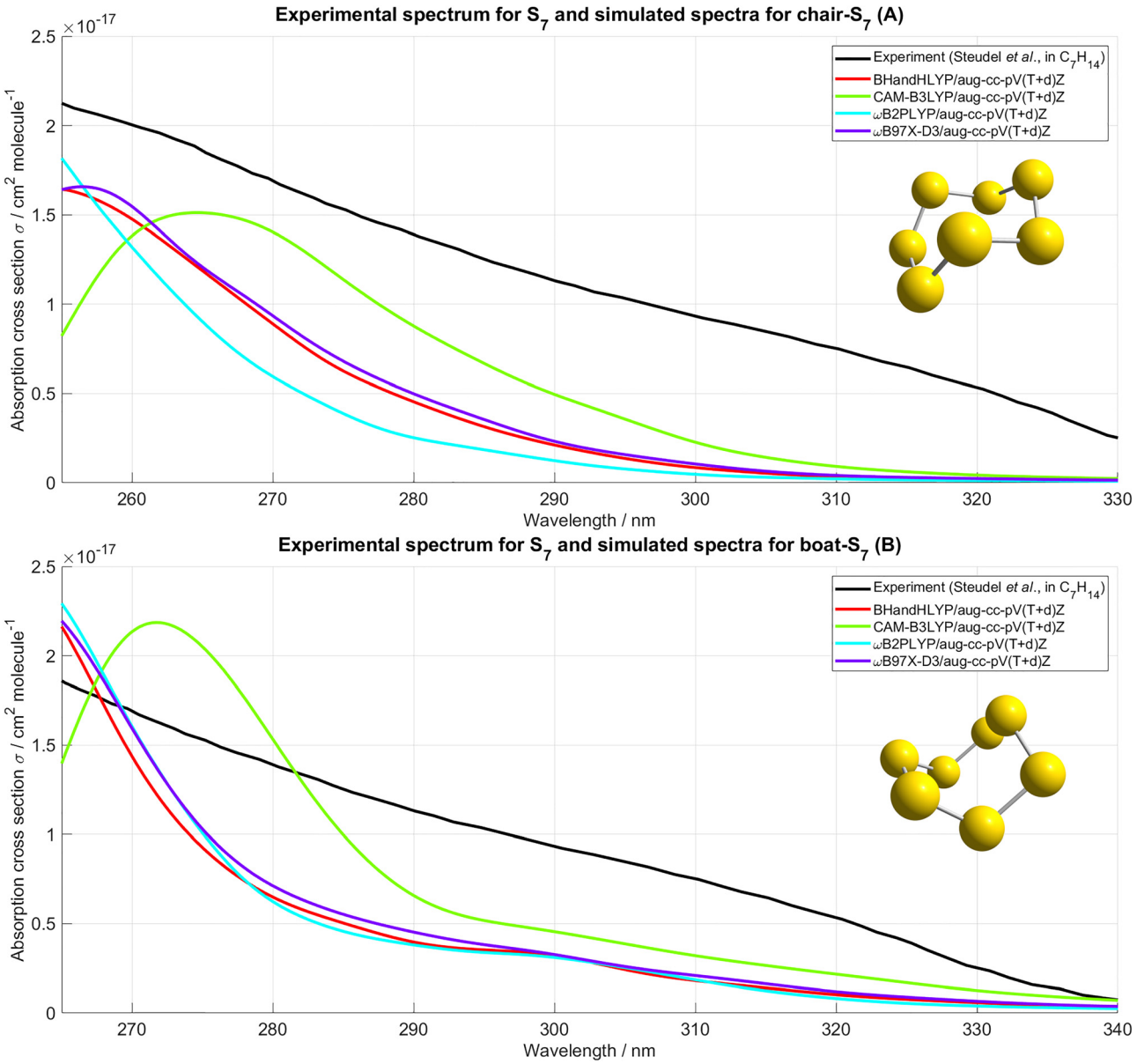

Fig. 11 The simulated spectra for the two lowest energy S_7 conformers, chair-S_7 and boat-S_7, compared to the experimental spectrum by Steudel *et al.*[53] measured in a methylcyclohexane (C_7H_{14}) solution. The experimental spectrum was digitized using the PlotDigitizer[134] tool. Note the different scales on the axes.

calculated including SOC. Furthermore, while including SOC allowed some triplet transitions to have nonzero oscillator strengths, the oscillator strengths were at least two orders of magnitude lower when compared to the singlet transitions. We therefore conclude that the effect of SOC is negligible.

Although S_8 was suggested as a possible UA candidate,[31] based on our simulated gas phase spectra crown-S_8 has no appreciable absorption cross section in the UA wavelength range of 320–400 nm. We therefore refute gas phase S_8 as an UA candidate.

4 Conclusions

In this work, we used the nuclear ensemble approximation approach to simulate UV-Vis spectra for the polysulfur species S_2–S_8. Our results provide wavelength-dependent absolute absorption cross sections for individual structural isomers, which can be included into photochemical models. Successful benchmark calculations using a set of small molecules and radicals (CS_2, H_2S, HO_2, O_3, OCS, PH_3, SO_2, and SO_3) indicate that the nuclear ensemble approach is a valid approach to simulate UV-Vis spectra.

Our results show that polysulfurs display great structural diversity. The lowest energy S_2–S_4 structures tend to be linear, while cyclic structures are the lowest energy structures for the larger S_5–S_8 species. Furthermore, we identified two low-energy triplet S_4 species, *cis*-$^3S_4$ and *trans*-$^3S_4$, that could be important intermediates in polysulfur reactions.

We recommend using the MC-RPA scaled EOM-CCSD/aug-cc-pV(T+d)Z spectra for linear-S_3, *cis*-S_4, and *trans*-S_4 when

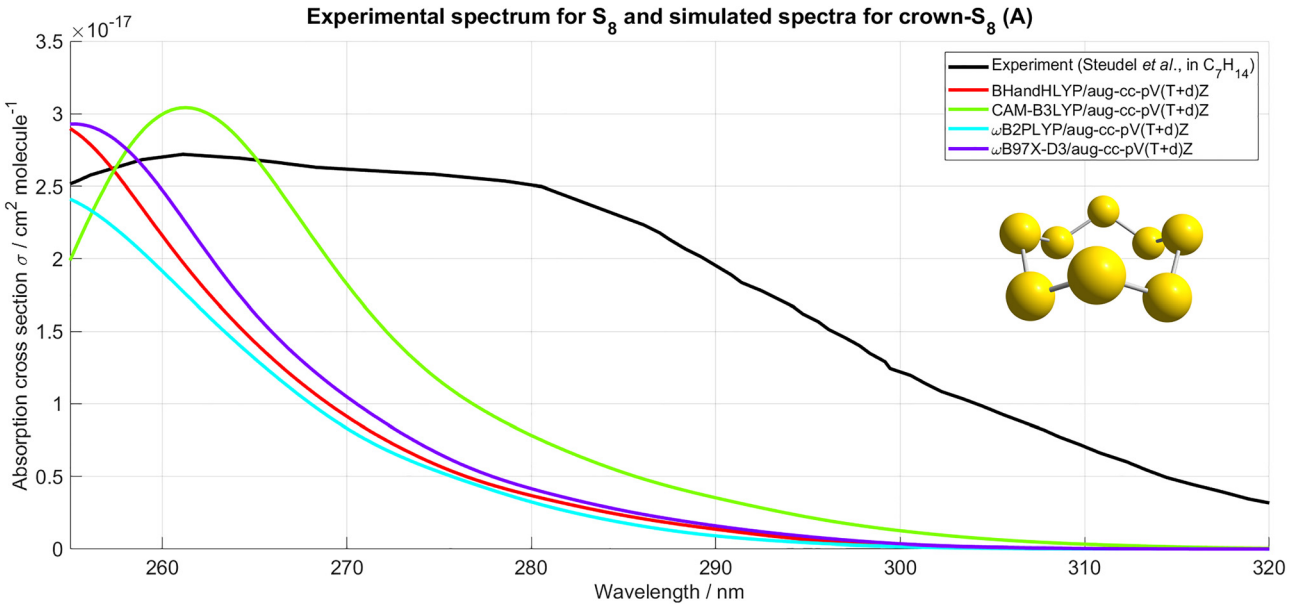

Fig. 12 The simulated spectra for crown-S_8, compared to the experimental spectrum by Steudel *et al.*[53] measured in a methylcyclohexane (C_7H_{14}) solution. The experimental spectrum was digitized using the PlotDigitizer[134] tool.

adding these species to photochemical models. For the other S_3 and S_4 species, the EOM-CCSD/aug-cc-pV(T+d)Z spectra are recommended. The ωB97X-D3/aug-cc-pV(T+d)Z spectra are recommended for the S_5–S_8 species. Finally, for S_2 we recommend using previously published experimental gas phase spectra or high-level simulated spectra.[48,60,61]

Based on the simulated spectra, we find two structures that absorb in the same wavelength region (320–400 nm) as the unknown absorber in the Venusian atmosphere, these being linear-S_3 and trigonal-S_4. However, the low concentrations predicted by Venusian atmospheric models makes it unlikely that polysulfurs are a major contributor to the enigmatic absorption. A conclusive assessment could be possible by investigating the accuracy of the polysulfur reaction rates used in Venusian atmospheric models, either using experimental methods or through high-level *ab initio* calculations.

For future work, the simulated spectra for the S_5–S_8 species should be extended down to 200 nm, as the high spectral resolution channel of the VenSpec-U UV-Vis spectrometer onboard the EnVision spacecraft reaches down to 205 nm.[137] Finally, with the upcoming mission to Venus by NASA (DAVINCI[138] and VERITAS[139]) and ESA (EnVision[140]), investigating sulfur chemistry in the context of Venus is vital for correctly interpreting the data these missions will produce in the coming decade.

Author contributions

R. S.: investigation; formal analysis; writing – original draft preparation; writing – review & editing; funding acquisition. B. N. F.: conceptualization; writing – review & editing; supervision; funding acquisition; project administration.

Conflicts of interest

There are no conflicts to declare.

Data availability

Supplementary information is available. See DOI: **https://doi.org/10.1039/d5cp02991k**.

Data supporting the findings in this article can be found in the SI. The simulated spectra for all species are included in the Zenodo archive DOI: **https://doi.org/10.5281/zenodo.16361268**.

Acknowledgements

R. S. acknowledges the support from the Doctoral Programme in Chemistry and Molecular Sciences (CHEMS-DP) at the University of Helsinki. R. S. thanks Dr Alyce Whipp and Mr Hugo Åström (University of Helsinki) for language edits, and Dr Nino Runeberg (CSC – IT Center for Science) and Prof. Sarai Dery Folkestad (Norwegian University of Science and Technology) for helping with the calculations. R. S. and B. N. F. thank Ms Nanna Falk Christensen for helpful discussions on spectral simulations. B. N. F. thanks for the fellowship support from the Carlsberg Foundation (CF22-0754) and the Magnus Ehrnrooth Foundation. The authors thank Prof. Theo Kurtén (University of Helsinki) for helpful discussions, and acknowledge Research Council of Finland Center of Excellence VILMA grant number 346369. Computational resources were generously provided by CSC – IT Center for Science (Espoo, Finland) project number 2008552.

References

1 D. V. Titov, H. Svedhem and F. W. Taylor, in *The Atmosphere of Venus: Current Knowledge and Future Investigations*, ed. P. Blondel and J. W. Mason, Springer-Verlag, Berlin, Heidelberg, 2006, pp. 87–110.

2 B. Fegley, *Treatise on Geochemistry*, Elsevier, Oxford, 2nd edn, 2014, pp. 127–148.

3 A. Vandaele, O. Korablev, D. Belyaev, S. Chamberlain, D. Evdokimova, T. Encrenaz, L. Esposito, K. Jessup, F. Lefèvre, S. Limaye, A. Mahieux, E. Marcq, F. Mills, F. Montmessin, C. Parkinson, S. Robert, T. Roman, B. Sandor, A. Stolzenbach, C. Wilson and V. Wilquet, *Icarus*, 2017, **295**, 16–33.

4 C. Gillmann, G. N. Arney, G. Avice, M. Dyar, G. J. Golabek, A. J. Gülcher, N. M. Johnson, M. Lefèvre and T. Widemann, *Treatise on Geochemistry*, Elsevier, Oxford, 3rd edn, 2025, pp. 289–323.

5 A. Mahieux, S. Robert, F. Mills, K. Jessup, L. Trompet, S. Aoki, A. Piccialli, J. Peralta and A. Vandaele, *Icarus*, 2023, **399**, 115556.

6 S.-M. Tsai, E. K. H. Lee, D. Powell, P. Gao, X. Zhang, J. Moses, E. Hébrard, O. Venot, V. Parmentier, S. Jordan, R. Hu, M. K. Alam, L. Alderson, N. M. Batalha, J. L. Bean, B. Benneke, C. J. Bierson, R. P. Brady, L. Carone, A. L. Carter, K. L. Chubb, J. Inglis, J. Leconte, M. Line, M. López-Morales, Y. Miguel, K. Molaverdikhani, Z. Rustamkulov, D. K. Sing, K. B. Stevenson, H. R. Wakeford, J. Yang, K. Aggarwal, R. Baeyens, S. Barat, M. De Val-Borro, T. Daylan, J. J. Fortney, K. France, J. M. Goyal, D. Grant, J. Kirk, L. Kreidberg, A. Louca, S. E. Moran, S. Mukherjee, E. Nasedkin, K. Ohno, B. V. Rackham, S. Redfield, J. Taylor, P. Tremblin, C. Visscher, N. L. Wallack, L. Welbanks, A. Youngblood, E.-M. Ahrer, N. E. Batalha, P. Behr, Z. K. Berta-Thompson, J. Blecic, S. L. Casewell, I. J. M. Crossfield, N. Crouzet, P. E. Cubillos, L. Decin, J.-M. Désert, A. D. Feinstein, N. P. Gibson, J. Harrington, K. Heng, T. Henning, E. M.-R. Kempton, J. Krick, P.-O. Lagage, M. Lendl, J. D. Lothringer, M. Mansfield, N. J. Mayne, T. Mikal-Evans, E. Palle, E. Schlawin, O. Shorttle, P. J. Wheatley and S. N. Yurchenko, *Nature*, 2023, **617**, 483–487.

7 A. Dyrek, M. Min, L. Decin, J. Bouwman, N. Crouzet, P. Mollière, P.-O. Lagage, T. Konings, P. Tremblin, M. Güdel, J. Pye, R. Waters, T. Henning, B. Vandenbussche, F. Ardevol Martinez, I. Argyriou, E. Ducrot, L. Heinke, G. Van Looveren, O. Absil, D. Barrado, P. Baudoz, A. Boccaletti, C. Cossou, A. Coulais, B. Edwards, R. Gastaud, A. Glasse, A. Glauser, T. P. Greene, S. Kendrew, O. Krause, F. Lahuis, M. Mueller, G. Olofsson, P. Patapis, D. Rouan, P. Royer, S. Scheithauer, I. Waldmann, N. Whiteford, L. Colina, E. F. Van Dishoeck, G. Östlin, T. P. Ray and G. Wright, *Nature*, 2024, **625**, 51–54.

8 T. G. Beatty, L. Welbanks, E. Schlawin, T. J. Bell, M. R. Line, M. Murphy, I. Edelman, T. P. Greene, J. J. Fortney, G. W. Henry, S. Mukherjee, K. Ohno, V. Parmentier, E. Rauscher, L. S. Wiser and K. E. Arnold, *Astrophys. J., Lett.*, 2024, **970**, L10.

9 A. Banerjee, J. K. Barstow, A. Gressier, N. Espinoza, D. K. Sing, N. H. Allen, S. M. Birkmann, R. C. Challener, N. Crouzet, C. A. Haswell, N. K. Lewis, S. R. Lewis and J. Yang, *Astrophys. J., Lett.*, 2024, **975**, L11.

10 N. Madhusudhan, S. Constantinou, M. Holmberg, S. Sarkar, A. A. A. Piette and J. I. Moses, *Astrophys. J., Lett.*, 2025, **983**, L40.

11 J. Pearl, R. Hanel, V. Kunde, W. Maguire, K. Fox, S. Gupta, C. Ponnamperuma and F. Raulin, *Nature*, 1979, **280**, 755–758.

12 J. R. Spencer, K. L. Jessup, M. A. McGrath, G. E. Ballester and R. Yelle, *Science*, 2000, **288**, 1208–1210.

13 S. Kremser, L. W. Thomason, M. Von Hobe, M. Hermann, T. Deshler, C. Timmreck, M. Toohey, A. Stenke, J. P. Schwarz, R. Weigel, S. Fueglistaler, F. J. Prata, J.-P. Vernier, H. Schlager, J. E. Barnes, J.-C. Antuña-Marrero, D. Fairlie, M. Palm, E. Mahieu, J. Notholt, M. Rex, C. Bingen, F. Vanhellemont, A. Bourassa, J. M. C. Plane, D. Klocke, S. A. Carn, L. Clarisse, T. Trickl, R. Neely, A. D. James, L. Rieger, J. C. Wilson and B. Meland, *Rev. Geophys.*, 2016, **54**, 278–335.

14 C. V. Brodowsky, T. Sukhodolov, G. Chiodo, V. Aquila, S. Bekki, S. S. Dhomse, M. Höpfner, A. Laakso, G. W. Mann, U. Niemeier, G. Pitari, I. Quaglia, E. Rozanov, A. Schmidt, T. Sekiya, S. Tilmes, C. Timmreck, S. Vattioni, D. Visioni, P. Yu, Y. Zhu and T. Peter, *Atmos. Chem. Phys.*, 2024, **24**, 5513–5548.

15 J. G. Calvert, A. Lazrus, G. L. Kok, B. G. Heikes, J. G. Walega, J. Lind and C. A. Cantrell, *Nature*, 1985, **317**, 27–35.

16 R. J. Weber, G. Chen, D. D. Davis, R. L. Mauldin III, D. J. Tanner, F. L. Eisele, A. D. Clarke, D. C. Thornton and A. R. Bandy, *J. Geophys. Res.:Atmos.*, 2001, **106**, 24107–24117.

17 M. Sipilä, T. Berndt, T. Petäjä, D. Brus, J. Vanhanen, F. Stratmann, J. Patokoski, R. L. Mauldin, A.-P. Hyvärinen, H. Lihavainen and M. Kulmala, *Science*, 2010, **327**, 1243–1246.

18 R. Zhang, A. Khalizov, L. Wang, M. Hu and W. Xu, *Chem. Rev.*, 2012, **112**, 1957–2011.

19 J. B. Pollack, O. B. Toon, R. C. Whitten, R. Boese, B. Ragent, M. Tomasko, L. Esposito, L. Travis and D. Wiedman, *J. Geophys. Res.:Space Phys.*, 1980, **85**, 8141–8150.

20 S. Pérez-Hoyos, A. Sánchez-Lavega, A. García-Muñoz, P. G. J. Irwin, J. Peralta, G. Holsclaw, W. M. McClintock and J. F. Sanz-Requena, *J. Geophys. Res.:Planets*, 2018, **123**, 145–162.

21 V. A. Krasnopolsky, *Photochemistry of the Atmospheres of Mars and Venus*, Springer Berlin Heidelberg, Berlin, Heidelberg, 1986, vol. 13.

22 L. Zasova, V. Krasnopolsky and V. Moroz, *Adv. Space Res.*, 1981, **1**, 13–16.

23 V. A. Krasnopolsky, *Icarus*, 2017, **286**, 134–137.

24 C. Z. Jiang, P. B. Rimmer, G. G. Lozano, N. J. Tosca, C. L. Kufner, D. D. Sasselov and S. J. Thompson, *Sci. Adv.*, 2024, **10**, eadg8826.

25 J. V. Egan, A. D. James and J. M. C. Plane, *ACS Earth Space Chem.*, 2025, **9**, 2127–2136.
26 T. Trabelsi and J. S. Francisco, *Astrophys. J.*, 2024, **977**, 92.
27 B. N. Frandsen, P. O. Wennberg and H. G. Kjaergaard, *Geophys. Res. Lett.*, 2016, **43**, 11146–11155.
28 B. N. Frandsen, S. Farahani, E. Vogt, J. R. Lane and H. G. Kjaergaard, *J. Phys. Chem. A*, 2020, **124**, 7047–7059.
29 J. Spacek, P. Rimmer, G. E. Owens, S. R. Cady, D. Sharma and S. A. Benner, *ACS Earth Space Chem.*, 2024, **8**, 89–98.
30 T. Trabelsi, *J. Phys. Chem. A*, 2025, **129**, 4870–4878.
31 B. Hapke and R. Nelson, *J. Atmos. Sci.*, 1975, **32**, 1212–1218.
32 O. B. Toon, R. P. Turco and J. B. Pollack, *Icarus*, 1982, **51**, 358–373.
33 V. Krasnopolsky, *Adv. Space Res.*, 1987, **7**, 25–27.
34 B. S. Maiorov, N. I. Ignat'ev, V. I. Moroz, L. V. Zasova, B. E. Moshkin, I. V. Khatuntsev and A. P. Ekonomov, *Sol. Syst. Res.*, 2005, **39**, 267–282.
35 V. A. Krasnopolsky, *Icarus*, 2013, **225**, 570–580.
36 F. P. Mills and M. Allen, *Planet. Space Sci.*, 2007, **55**, 1729–1740.
37 X. Zhang, M. C. Liang, F. P. Mills, D. A. Belyaev and Y. L. Yung, *Icarus*, 2012, **217**, 714–739.
38 V. A. Krasnopolsky, *Icarus*, 2012, **218**, 230–246.
39 A. Stolzenbach, F. Lefèvre, S. Lebonnois and A. Määttänen, *Icarus*, 2023, **395**, 115447.
40 C. J. Bierson and X. Zhang, *J. Geophys. Res.:Planets*, 2020, **125**, e2019JE006159.
41 P. B. Rimmer, S. Jordan, T. Constantinou, P. Woitke, O. Shorttle, R. Hobbs and A. Paschodimas, *Planet. Sci. J.*, 2021, **2**, 133.
42 A. Francés-Monerris, J. Carmona-García, T. Trabelsi, A. Saiz-Lopez, J. R. Lyons, J. S. Francisco and D. Roca-Sanjuán, *Nat. Commun.*, 2022, **13**, 4425.
43 J. I. Graham and W. N. Hartley, *Proc. R. Soc. London, Ser. A*, 1910, **84**, 311–324.
44 G. Herzberg and L. G. Mundie, *J. Chem. Phys.*, 1940, **8**, 263–273.
45 L. Brewer, G. D. Brabson and B. Meyer, *J. Chem. Phys.*, 1965, **42**, 1385–1389.
46 A. Kumar, P. Chowdhury, K. Rama Rao and J. Mittal, *Chem. Phys. Lett.*, 1992, **198**, 406–412.
47 J. Lindner, R. Niemann and E. Tiemann, *J. Mol. Spectrosc.*, 1994, **165**, 358–367.
48 G. Stark, H. Herde, J. R. Lyons, A. N. Heays, N. de Oliveira, G. Nave, B. R. Lewis and S. T. Gibson, *J. Chem. Phys.*, 2018, **148**, 244302.
49 B. Meyer, T. Stroyer-Hansen and T. Oommen, *J. Mol. Spectrosc.*, 1972, **42**, 335–343.
50 R. I. Billmers and A. L. Smith, *J. Phys. Chem.*, 1991, **95**, 4242–4245.
51 P. Hassanzadeh and L. Andrews, *J. Phys. Chem.*, 1992, **96**, 6579–6585.
52 M. S. Boumedien, J. Corset and E. Picquenard, *J. Raman Spectrosc.*, 1999, **30**, 463–472.
53 R. Steudel, D. Jensen, P. Göbel and P. Hugo, *Ber. Bunsen-Ges. Phys. Chem.*, 1988, **92**, 118–122.
54 W. C. Swope, Y. Lee, I. Schaefer and F. Henry, *J. Chem. Phys.*, 1979, **70**, 947–953.
55 G. Theodorakopoulos, S. Peyerimhoff and R. J. Buenker, *Chem. Phys. Lett.*, 1981, **81**, 413–420.
56 B. A. Hess, R. J. Buenker, C. M. Marian and S. D. Peyerimhoff, *Chem. Phys.*, 1982, **71**, 79–85.
57 T. Kiljunen, J. Eloranta, H. Kunttu, L. Khriachtchev, M. Pettersson and M. Räsänen, *J. Chem. Phys.*, 2000, **112**, 7475–7483.
58 W. Xing, D. Shi, J. Sun, H. Liu and Z. Zhu, *Mol. Phys.*, 2013, **111**, 673–685.
59 W. Xing, D. Shi and J. Sun, *J. Quant. Spectrosc. Radiat. Transfer*, 2020, **242**, 106805.
60 K. Sarka, S. O. Danielache, A. Kondorskiy and S. Nanbu, *Chem. Phys.*, 2019, **516**, 108–115.
61 K. Sarka and S. Nanbu, *ACS Earth Space Chem.*, 2023, **7**, 2374–2381.
62 K. A. Peterson, J. R. Lyons and J. S. Francisco, *J. Chem. Phys.*, 2006, **125**, 084314.
63 M. W. Wong and R. Steudel, *Chem. Phys. Lett.*, 2003, **379**, 162–169.
64 D. Hohl, R. O. Jones, R. Car and M. Parrinello, *J. Chem. Phys.*, 1988, **89**, 6823–6835.
65 G. E. Quelch, H. F. I. Schaefer and C. J. Marsden, *J. Am. Chem. Soc.*, 1990, **112**, 8719–8733.
66 K. Raghavachari, C. M. Rohlfing and J. S. Binkley, *J. Chem. Phys.*, 1990, **93**, 5862–5874.
67 M. Chen, M. Liu, H. Luo, Q. Zhang and C. Au, *J. Mol. Struct. THEOCHEM*, 2001, **548**, 133–141.
68 J. Cioslowski, A. Szarecka and D. Moncrieff, *J. Phys. Chem. A*, 2001, **105**, 501–505.
69 S. Millefiori and A. Alparone, *J. Phys. Chem. A*, 2001, **105**, 9489–9497.
70 M. W. Wong, Y. Steudel and R. Steudel, *Chem. Phys. Lett.*, 2002, **364**, 387–392.
71 R. O. Jones and P. Ballone, *J. Chem. Phys.*, 2003, **118**, 9257–9265.
72 M. H. Matus, D. A. Dixon, K. A. Peterson, J. A. W. Harkless and J. S. Francisco, *J. Chem. Phys.*, 2007, **127**, 174305.
73 C. Tian, Z. Wang, S. Pan, W. Zhao, Q. Guo and M. Jin, *J. Mol. Struct. THEOCHEM*, 2009, **906**, 1–5.
74 S. Farahani, B. N. Frandsen, H. G. Kjaergaard and J. R. Lane, *J. Phys. Chem. A*, 2019, **123**, 6605–6617.
75 M. Barbatti, A. J. A. Aquino and H. Lischka, *Phys. Chem. Chem. Phys.*, 2010, **12**, 4959–4967.
76 O. Ferchichi, N. Derbel, T. Cours and A. Alijah, *Phys. Chem. Chem. Phys.*, 2020, **22**, 4059–4071.
77 W. Chao, R. Skog, B. N. Frandsen, G. H. Jones, K. T. Pham, M. Okumura, M. P. Sulbaek Andersen, C. J. Percival and F. A. F. Winiberg, *Commun. Chem.*, 2025, **8**, 163.
78 A. Saiz-Lopez, S. P. Sitkiewicz, D. Roca-Sanjuán, J. M. Oliva-Enrich, J. Z. Dávalos, R. Notario, M. Jiskra, Y. Xu, F. Wang, C. P. Thackray, E. M. Sunderland, D. J. Jacob, O. Travnikov, C. A. Cuevas, A. U. Acuña, D. Rivero, J. M. C. Plane, D. E. Kinnison and J. E. Sonke, *Nat. Commun.*, 2018, **9**, 4796.

79 M. Barbatti and K. Sen, *Int. J. Quantum Chem.*, 2016, **116**, 762–771.
80 A. Prlj, E. Marsili, L. Hutton, D. Hollas, D. Shchepanovska, D. R. Glowacki, P. Slavícek and B. F. E. Curchod, *ACS Earth Space Chem.*, 2022, **6**, 207–217.
81 A. Prlj, D. Hollas and B. F. E. Curchod, *J. Phys. Chem. A*, 2023, **127**, 7400–7409.
82 D. Hollas and B. F. E. Curchod, *J. Phys. Chem. A*, 2024, **128**, 8580–8590.
83 H. Keller-Rudek, G. K. Moortgat, R. Sander and R. Sörensen, *Earth Syst. Sci. Data*, 2013, **5**, 365–373.
84 D. A. Matthews, L. Cheng, M. E. Harding, F. Lipparini, S. Stopkowicz, T.-C. Jagau, P. G. Szalay, J. Gauss and J. F. Stanton, *J. Chem. Phys.*, 2020, **152**, 214108.
85 J. F. Stanton, J. Gauss, L. Cheng, M. E. Harding, D. A. Matthews and P. G. Szalay, CFOUR, Coupled-Cluster techniques for Computational Chemistry, a quantum-chemical program package, with contributions from A. Asthana, A.A. Auer, R.J. Bartlett, U. Benedikt, C. Berger, D.E. Bernholdt, S. Blaschke, Y. J. Bomble, S. Burger, O. Christiansen, D. Datta, F. Engel, R. Faber, J. Greiner, M. Heckert, O. Heun, M. Hilgenberg, C. Huber, T.-C. Jagau, D. Jonsson, J. Jusélius, T. Kirsch, M.-P. Kitsaras, K. Klein, G.M. Kopper, W.J. Lauderdale, F. Lipparini, J. Liu, T. Metzroth, L. Monzel, L.A. Mück, D.P. O'Neill, T. Nottoli, J. Ostwald, D. R. Price, E. Prochnow, C. Puzzarini, K. Ruud, F. Schiffmann, W. Schwalbach, C. Simmons, S. Stopkowicz, A. Tajti, T. Uhlířová, J. Vázquez, F. Wang, J. D. Watts, P. Yergün. C. Zhang, X. Zheng, and the integral packages MOLECULE (J. Almlöf and P. R. Taylor), PROPS (P. R. Taylor), ABACUS (T. Helgaker, H. J. Aa. Jensen, P. Jørgensen, and J. Olsen), and ECP routines by A. V. Mitin and C. van Wüllen, For the current version, see **https://www.cfour.de**.
86 A. D. Becke, *J. Chem. Phys.*, 1993, **98**, 1372–1377.
87 T. Yanai, D. P. Tew and N. C. Handy, *Chem. Phys. Lett.*, 2004, **393**, 51–57.
88 Y.-S. Lin, G.-D. Li, S.-P. Mao and J.-D. Chai, *J. Chem. Theory Comput.*, 2013, **9**, 263–272.
89 M. Casanova-Páez, M. B. Dardis and L. Goerigk, *J. Chem. Theory Comput.*, 2019, **15**, 4735–4744.
90 J. Dunning and H. Thom, *J. Chem. Phys.*, 1989, **90**, 1007–1023.
91 J. Dunning, H. Thom, K. A. Peterson and A. K. Wilson, *J. Chem. Phys.*, 2001, **114**, 9244–9253.
92 R. A. Kendall, J. Dunning, H. Thom and R. J. Harrison, *J. Chem. Phys.*, 1992, **96**, 6796–6806.
93 D. E. Woon, J. Dunning and H. Thom, *J. Chem. Phys.*, 1993, **98**, 1358–1371.
94 M. J. Frisch, G. W. Trucks, H. B. Schlegel, G. E. Scuseria, M. A. Robb, J. R. Cheeseman, G. Scalmani, V. Barone, G. A. Petersson, H. Nakatsuji, X. Li, M. Caricato, A. V. Marenich, J. Bloino, B. G. Janesko, R. Gomperts, B. Mennucci, H. P. Hratchian, J. V. Ortiz, A. F. Izmaylov, J. L. Sonnenberg, D. Williams-Young, F. Ding, F. Lipparini, F. Egidi, J. Goings, B. Peng, A. Petrone, T. Henderson, D. Ranasinghe, V. G. Zakrzewski, J. Gao, N. Rega, G. Zheng, W. Liang, M. Hada, M. Ehara, K. Toyota, R. Fukuda, J. Hasegawa, M. Ishida, T. Nakajima, Y. Honda, O. Kitao, H. Nakai, T. Vreven, K. Throssell, J. A. Montgomery, Jr., J. E. Peralta, F. Ogliaro, M. J. Bearpark, J. J. Heyd, E. N. Brothers, K. N. Kudin, V. N. Staroverov, T. A. Keith, R. Kobayashi, J. Normand, K. Raghavachari, A. P. Rendell, J. C. Burant, S. S. Iyengar, J. Tomasi, M. Cossi, J. M. Millam, M. Klene, C. Adamo, R. Cammi, J. W. Ochterski, R. L. Martin, K. Morokuma, O. Farkas, J. B. Foresman and D. J. Fox, *Gaussian 16 Revision C.02*, Gaussian Inc., Wallingford CT, 2021.
95 F. Neese, *Wiley Interdiscip. Rev.:Comput. Mol. Sci.*, 2022, **12**, e1606.
96 B. P. Pritchard, D. Altarawy, B. Didier, T. D. Gibson and T. L. Windus, *J. Chem. Inf. Model.*, 2019, **59**, 4814–4820.
97 R. Crespo-Otero and M. Barbatti, *Theor. Chem. Acc.*, 2012, **131**, 1237.
98 R. Crespo-Otero and M. Barbatti, *Chem. Rev.*, 2018, **118**, 7026–7068.
99 M. Barbatti, M. Bondanza, R. Crespo-Otero, B. Demoulin, P. O. Dral, G. Granucci, F. Kossoski, H. Lischka, B. Mennucci, S. Mukherjee, M. Pederzoli, M. Persico, M. Pinheiro Jr, J. Pittner, F. Plasser, E. Sangiogo Gil and L. Stojanovic, *J. Chem. Theory Comput.*, 2022, **18**, 6851–6865.
100 M. Barbatti, G. Granucci, M. Ruckenbauer, F. Plasser, R. Crespo-Otero, J. Pittner, M. Persico and H. Lischka, NEWTON-X: a package for Newtonian dynamics close to the crossing seam, version 2.6 build *01*, 2023, **https://www.newtonx.org**.
101 S. Mai, H. Gattuso, A. Monari and L. González, *Front. Chem.*, 2018, **6**, 495.
102 MATLAB, version: 24.1.0.2653294 (R2024a) Update 5, 2024, The MathWorks Inc., Natick, Massachusetts, **https://www.mathworks.com**.
103 P. Pracht, F. Bohle and S. Grimme, *Phys. Chem. Chem. Phys.*, 2020, **22**, 7169–7192.
104 P. Pracht, S. Grimme, C. Bannwarth, F. Bohle, S. Ehlert, G. Feldmann, J. Gorges, M. Müller, T. Neudecker, C. Plett, S. Spicher, P. Steinbach, P. A. Wesolowski and F. Zeller, *J. Chem. Phys.*, 2024, **160**, 114110.
105 C. Bannwarth, S. Ehlert and S. Grimme, *J. Chem. Theory Comput.*, 2019, **15**, 1652–1671.
106 M. S. Gordon, J. S. Binkley, J. A. Pople, W. J. Pietro and W. J. Hehre, *J. Am. Chem. Soc.*, 1982, **104**, 2797–2803.
107 J.-D. Chai and M. Head-Gordon, *J. Chem. Phys.*, 2008, **128**, 084106.
108 J.-D. Chai and M. Head-Gordon, *Phys. Chem. Chem. Phys.*, 2008, **10**, 6615–6620.
109 E. Miliordos and S. S. Xantheas, *J. Am. Chem. Soc.*, 2014, **136**, 2808–2817.
110 D. Mester, P. R. Nagy, J. Csóka, L. Gyevi-Nagy, P. B. Szabó, R. A. Horváth, K. Petrov, B. Hégely, B. Ladóczki, G. Samu, B. D. Lorincz and M. Kállay, *J. Phys. Chem. A*, 2025, **129**, 2086–2107.
111 F. Neese, *Wiley Interdiscip. Rev.:Comput. Mol. Sci.*, 2025, **15**, e70019.

112 H. Grosch, A. Fateev and S. Clausen, *J. Quant. Spectrosc. Radiat. Transfer*, 2015, **154**, 28–34.
113 K. Sunanda, A. Shastri, A. K. Das and B. Raja Sekhar, *J. Quant. Spectrosc. Radiat. Transfer*, 2015, **151**, 76–87.
114 J. W. Rabalais, J. R. McDonald, V. M. Scherr and S. P. McGlynn, *Chem. Rev.*, 1971, **71**, 73–108.
115 C. Wu and F. Chen, *J. Quant. Spectrosc. Radiat. Transfer*, 1998, **60**, 17–23.
116 S. P. Sander, J. Abbatt, J. R. Barker, J. B. Burkholder, R. R. Friedl, D. M. Golden, R. E. Huie, C. E. Kolb, M. J. Kurylo, G. K. Moortgat, V. L. Orkin and P. H. Wine, Chemical Kinetics and Photochemical Data for Use in Atmospheric Studies, Evaluation No. 17, JPL Publication 10-6, Jet Propulsion Laboratory, Pasadena, 2011, **https://jpldataeval.jpl.nasa.gov**.
117 P. Limão-Vieira, F. Ferreira da Silva, D. Almeida, M. Hoshino, H. Tanaka, D. Mogi, T. Tanioka, N. J. Mason, S. V. Hoffmann, M.-J. Hubin-Franskin and J. Delwiche, *J. Chem. Phys.*, 2015, **142**, 064303.
118 F. Chen, D. L. Judge, C. Y. Robert Wu, J. Caldwell, H. P. White and R. Wagener, *J. Geophys. Res.:Planets*, 1991, **96**, 17519–17527.
119 S. L. Manatt and A. L. Lane, *J. Quant. Spectrosc. Radiat. Transfer*, 1993, **50**, 267–276.
120 J. B. Burkholder and S. McKeen, *Geophys. Res. Lett.*, 1997, **24**, 3201–3204.
121 P. E. Hintze, H. G. Kjaergaard, V. Vaida and J. B. Burkholder, *J. Phys. Chem. A*, 2003, **107**, 1112–1118.
122 I. Barnes, K. Becker and E. Fink, *Chem. Phys. Lett.*, 1979, **67**, 314–317.
123 L. Xiao, B. Yan and B. F. Minaev, *Physchem*, 2023, **3**, 110–124.
124 M. C. McCarthy, S. Thorwirth, C. A. Gottlieb and P. Thaddeus, *J. Am. Chem. Soc.*, 2004, **126**, 4096–4097.
125 S. Thorwirth, M. C. McCarthy, C. A. Gottlieb, P. Thaddeus, H. Gupta and J. F. Stanton, *J. Chem. Phys.*, 2005, **123**, 054326.
126 B. Flemmig, P. T. Wolczanski and R. Hoffmann, *J. Am. Chem. Soc.*, 2005, **127**, 1278–1285.
127 J. Ivanic, G. J. Atchity and K. Ruedenberg, *J. Chem. Phys.*, 1997, **107**, 4307–4317.
128 J. D. Goddard, X. Chen and G. Orlova, *J. Phys. Chem. A*, 1999, **103**, 4078–4084.
129 B. Helmich-Paris, *J. Chem. Phys.*, 2019, **150**, 174121.
130 A. D. Torres, M. A. S. Francisco, R. R. Oliveira and A. B. Rocha, *J. Phys. Chem. A*, 2023, **127**, 3200–3209.
131 S. D. Folkestad, E. F. Kjønstad, R. H. Myhre, J. H. Andersen, A. Balbi, S. Coriani, T. Giovannini, L. Goletto, T. S. Haugland, A. Hutcheson, I.-M. Høyvik, T. Moitra, A. C. Paul, M. Scavino, A. S. Skeidsvoll, S. H. Tveten and H. Koch, *J. Chem. Phys.*, 2020, **152**, 184103.
132 S. Du, T. C. Germann, J. S. Francisco, K. A. Peterson, H.-G. Yu and J. R. Lyons, *J. Chem. Phys.*, 2011, **134**, 154508.
133 J. I. Moses, M. Y. Zolotov and B. Fegley, *Icarus*, 2002, **156**, 76–106.
134 *PlotDigitizer: Version 3.1.6*, PORBITAL Technologies, 2025, **https://plotdigitizer.com**.
135 R. O. Jones and D. Hohl, *Int. J. Quantum Chem.*, 1990, **38**, 141–151.
136 B. de Souza, G. Farias, F. Neese and R. Izsák, *J. Chem. Theory Comput.*, 2019, **15**, 1896–1904.
137 E. Marcq, F. Montmessin, J. Lasue, B. Bézard, K. L. Jessup, Y. J. Lee, C. F. Wilson, B. Lustrement, N. Rouanet and G. Guignan, *Adv. Space Res.*, 2021, **68**, 275–291.
138 J. B. Garvin, S. A. Getty, G. N. Arney, N. M. Johnson, E. Kohler, K. O. Schwer, M. Sekerak, A. Bartels, R. S. Saylor, V. E. Elliott, C. S. Goodloe, M. B. Garrison, V. Cottini, N. Izenberg, R. Lorenz, C. A. Malespin, M. Ravine, C. R. Webster, D. H. Atkinson, S. Aslam, S. Atreya, B. J. Bos, W. B. Brinckerhoff, B. Campbell, D. Crisp, J. R. Filiberto, F. Forget, M. Gilmore, N. Gorius, D. Grinspoon, A. E. Hofmann, S. R. Kane, W. Kiefer, S. Lebonnois, P. R. Mahaffy, A. Pavlov, M. Trainer, K. J. Zahnle and M. Zolotov, *Planet. Sci. J.*, 2022, **3**, 117.
139 G. Cascioli, S. Hensley, F. De Marchi, D. Breuer, D. Durante, P. Racioppa, L. Iess, E. Mazarico and S. E. Smrekar, *Planet. Sci. J.*, 2021, **2**, 220.
140 R. Ghail, C. Wilson, T. Widemann, L. Bruzzone, C. Dumoulin, J. Helbert, R. Herrick, E. Marcq, P. Mason, P. Rosenblatt, A. C. Vandaele and L.-J. Burtz, EnVision: understanding why our most Earth-like neighbour is different, *arXiv*, 2017, preprint, arXiv:1703.09010, DOI: **10.48550/arXiv.1703.09010**.